# Two Components of Voltage-Dependent Inactivation in $Ca_v1.2$ Channels Revealed by Its Gating Currents

Gonzalo Ferreira,* Eduardo Ríos,† and Nicolás Reyes*
*Departmento Biofísica, Facultad de Medicina, Montevideo, Uruguay; and †Department of Molecular Biophysics and Physiology, Rush University, Chicago, Illinois USA

ABSTRACT Voltage-dependent inactivation (VDI) was studied through its effects on the voltage sensor in $Ca_v1.2$ channels expressed in tsA 201 cells. Two kinetically distinct phases of VDI in onset and recovery suggest the presence of dual VDI processes. Upon increasing duration of conditioning depolarizations, the half-distribution potential ($V_{1/2}$) of intramembranous mobile charge was negatively shifted as a sum of two exponential terms, with time constants 0.5 s and 4 s, and relative amplitudes near 50% each. This kinetics behavior was consistent with that of increment of maximal charge related to inactivation (*Qn*). Recovery from inactivation was also accompanied by a reduction of *Qn* that varied with recovery time as a sum of two exponentials. The amplitudes of corresponding exponential terms were strongly correlated in onset and recovery, indicating that channels recover rapidly from fast VDI and slowly from slow VDI. Similar to charge "immobilization," the charge moved in the repolarization (*OFF*) transient became slower during onset of fast VDI. Slow VDI had, instead, hallmarks of interconversion of charge. Confirming the mechanistic duality, fast VDI virtually disappeared when $Li^+$ carried the current. A nine-state model with parallel fast and slow inactivation pathways from the open state reproduces most of the observations.

## INTRODUCTION

Inactivation, a process that puts channels in closed unresponsive states, and usually occurs after activation, is a widespread and prominent characteristic of ion channels. It has major physiological importance, as it controls the duration of phenomena such as action potentials (by affecting voltage-operated channels) and excitation-contraction coupling (affecting, in this case, intracellular $Ca^{2+}$ release channels).

In cardiac L-type $Ca^{2+}$ channels, inactivation can be driven, in addition to voltage, by the passage of current (current-dependent inactivation, or CDI). CDI is characterized by a U-shaped dependence on conditioning voltage and by additional dependence on the permeant ion species. Its structural underpinnings comprise the action of constitutively bound calmodulin to the channel, which either inactivates or potentiates the channel upon $Ca^{2+}$ binding (Peterson et al., 1999, 2000; Qin et al., 1999; Zuhlke et al., 1999; Erickson et al., 2001, Mouton et al., 2001). Voltage-dependent inactivation (VDI) of L-type $Ca^{2+}$ channels has been studied comparatively less than their CDI. Based on the kinetics of decay of $Ba^{2+}$ currents, fast and slow VDI mechanisms have been proposed (Kass and Sanguinetti, 1984; Hering et al., 2000; Stotz and Zamponi, 2001a). Additionally, from the changes in the kinetics of decay of $Ba^{2+}$ currents in mutants of intracellular regions of $Ca^{2+}$ channels, a hinged-lid mechanism has been suggested (Bernatchez et al., 1998; Cens et al., 1999; Stotz et al., 2000; Stotz and Zamponi, 2001a). Because of the direct effects of $Ba^{2+}$ on inactivation, however, a description of VDI in isolation can only be drawn from studies of gating currents (Ferreira et al., 1997b). Though part of these studies have been made in native cells, they face the problem of heterogeneity of gating currents as cardiac L-type $Ca^{2+}$ channels coexist with other voltage-dependent channels, which contribute their own gating current. Because of these problems, we took advantage of characterizing VDI in expressed cardiac L-type $Ca^{2+}$ channels in tsA 201 cells, which are virtually devoid of intrinsic voltage-dependent channels that could interfere in the measurements of gating currents.

A variety of inactivation phenomena have been described for voltage-dependent channels, on a wide range of timescales, from milliseconds to seconds. Different mechanisms have been characterized initially by the presence of fast (milliseconds) and slow (seconds) time constants in their onset and recovery. For some mechanisms, the structural underpinnings are clearly identified, while in others molecular identification has just begun. One aim of the present work is to probe the existence of multiple kinetic components of VDI in cardiac L-type $Ca^{2+}$ channels, through the study of changes in gating currents during inactivation.

At the level of the voltage sensor, inactivation in voltage-dependent channels is associated with charge ''immobilization'' and/or charge interconversion. Charge immobilization has been described in fast inactivation of voltage-dependent $Na^+$ and *Shaker* $K^+$ channels (N-type) (Armstrong and Bezanilla, 1977; Bezanilla et al., 1991; Bezanilla, 2000). The main hallmark of charge immobilization is the slowing of the voltage sensor movement upon repolarization, which leads to the reduction of the charge measured at the trailing edge of the depolarization that caused inactivation ($Q_{OFF}$) (Armstrong and Bezanilla, 1977; Yellen, 1998; Bezanilla, 2000). Charge thus immobilized recovers (remobilizes) with a steep voltage-dependence, becoming available to move in a new

*Submitted June 25, 2002, and accepted for publication December 26, 2002.*
Address reprint requests to Gonzalo Ferreira, Departmento Biofísica, Facultad de Medicina, Gral. Flores 2125, CP11800, Montevideo, Uruguay. E-mail: ferreira@fmed.edu.uy.

0006-3495/03/06/3662/17 $2.00

depolarization. This remobilization manifests itself as a slow component of $Q_{OFF}$. Because the kinetics behavior of this slow component becomes similar to that of the regular, not-immobilized charge at large hyperpolarizations, the effect differs from the shift of the *Q-V* curve that follows charge interconversion (discussed below). In other words, when recovery from inactivation is fast and limited by the movement of the voltage sensor itself, the result is charge immobilization. Schematically, charge immobilization has been pictured as the result of a ball-and-chain or a hinged-lid mechanism in which the internal mouth of the pore is occluded by a cytoplasmic moiety of the channel (Armstrong and Bezanilla, 1977; Hoshi et al., 1990; Bezanilla et al., 1991; Eaholtz et al., 1994; Yellen, 1998; Bezanilla, 2000). The binding of the particle to the channel retards the return of the voltage sensor, leading to immobilization of charge. A second aim of the present work is to look for a phenomenologically similar mechanism in $Ca_v1.2$ channels, by studying their gating currents in tsA 201 cells.

Charge interconversion, implied in a model by Bezanilla et al. (1982) to explain long-term inactivation of $Na^+$ channel gating currents, has been described in the DHP receptor of skeletal muscle and L-type $Ca^{2+}$ channels in native cardiac muscle (Brum and Rios, 1987; Shirokov et al., 1992; Josephson, 1996; Ferreira et al., 1997a; Shirokov et al., 1998). During activation the charge moves between its *cis* (inner) and *trans* (outer) positions, with half-distribution potential ($V_{1/2}$) near 0 mV in expressed $Ca_v1.2$ (Shirokov et al., 1998). This mode of charge movement, associated with activation and deactivation of the skeletal and cardiac L-type $Ca^{2+}$ channels, has been termed Charge 1. The signature of charge interconversion is the possibility of return of the mobile charge to a *cis* position before recovery from inactivation. The intramembranous charge remains mobile between its *cis* and *trans* positions, but it is voltage-shifted, with $V_{1/2}$ near $-90$ mV (Shirokov et al., 1998). This second mode of charge movement, which takes place within inactivated channels, has been termed Charge 2. Otherwise stated, this form of inactivation, which is slow in onset and recovery, seems to have its recovery limited intrinsically, by a step that is not associated with measurable intramembranous charge movement. Consequently, charge can be moved back and forth among inactivated states and one can speak of charge interconversion between a mode that moves ineffectually among inactivated states, i.e., Charge 2, and a normal or reprimed mode, Charge 1. Charge interconversion shares properties with changes in gating currents associated with slow inactivation of voltage-dependent $Na^+$ and $K^+$ channels (Bezanilla et al., 1982; Starkus and Rayner, 1991; Olcese et al., 1997). The structural basis of slow inactivation in these channels is not elucidated, though it may be related to changes in the whole channel, particularly in the pore and outer vestibule (Yellen et al., 1994; Baukrowitz and Yellen, 1995; Loots and Isacoff, 1998; Bezanilla, 2000; Vilin et al., 1999; Ong et al., 2000). We have previously reported some of the characteristics of charge interconversion in expressed $Ca_v1.2$ (Shirokov et al., 1998). In this article, we explore its kinetic aspects in further detail.

Extracellular ions alter inactivation in different ways. Usually, higher occupancy of the ion binding site/s related to inactivation delays its onset (though the converse case has also been described; see De Biasi et al., 1993; Yellen, 1998). In *Shaker* and other voltage-dependent $K^+$ channels, slow inactivation includes a variety of mechanisms (termed C, P, and U-type inactivation), which are all modulated by the nature and concentration of the ions present in the extracellular solutions (Hoshi et al., 1991; Lopez-Barneo et al., 1993; De Biasi et al., 1993; Olcese et al., 1997; Klemic et al., 2001). Taking into account these reports, we also tested whether extracellular cations modulate gating current changes associated with inactivation in expressed $Ca_v1.2$ channels.

In this article, we biophysically characterize VDI by studying gating currents in L-type cardiac $Ca^{2+}$ channels ($Ca_v1.2$) expressed in tsA201 cells. The results are consistent with the presence of two distinct processes: one is fast, and involves charge immobilization; the other is slow, and results in charge interconversion. Interestingly, the presence of divalent (or trivalent) cations in the extracellular solution appears to be required for the development of the fast inactivation process.

## METHODS

Experiments were done with the tsA201 cell line (large T-antigen-transformed human embryonic kidney). Cells were grown in DME medium supplemented with 10% FBS, 100 U/ml penicillin, and 0.1 mg/ml streptomycin (Sigma Chemical, St. Louis, MO) in 5% $CO_2$. Cardiac rabbit $\alpha_{1C}$, rat brain $\beta_{2a}$, and rabbit skeletal muscle $\alpha_2\delta$ cDNAs, were cloned in pCR3, pCMV, and pMT2 plasmid vectors, respectively. High purity ($A_{260}/A_{280} \geq 1.95$) large-scale plasmid preparations were obtained using standard protocols (Qiagen, Chadworth, CA). Transfections were done with 6 $\mu$g of each expression plasmid in 60-mm dishes using a modified calcium phosphate precipitation method. Electrophysiological recordings were made within 24–48 h posttransfection on round nonclustered cells. No sizable ionic or gating currents were observed in tsA201 cells in the absence of transfection. After transfection, the fraction of cells selected and patched that had $Ca^{2+}$ currents was 40–60%.

Cells were placed in a small chamber and perfused by continuous flow of external solutions. Records were obtained by a standard whole-cell patch-clamp procedure using an Axopatch 200B amplifier (Axon Instruments, Foster City, CA) and a 16-bit A/D–D/A converter card (HSDAS 16, Analogic, Peabody, MA) on a PC computer. Ionic currents were sampled at 1–3 kHz and gating currents (detailed below) at 10–40 kHz, depending on pulse duration.

The internal solution contained (in mM): 150 CsOH (or NMG), 110 Glutamate, 20 HCl, 10 HEPES, 5 MgATP, and 10 EGTA (pH adjusted to 7.6 by addition of CsOH). Osmolality of the internal solution was routinely measured and adjusted to 300–320 mosmole/Kg. External recording solutions contained (in mM): 140 TEA-Cl, 10 Tris, and either 10 $CaCl_2$ or 10 $BaCl_2$. Lithium external solution contained (in mM): 150 LiCl, 10 HEPES. In some experiments, 0.5 $\mu$M $CaCl_2$ was added to this solution to stabilize the patch seal. In gating current experiments, 10–20 $\mu$M $GdCl_3$ was

added to the external solution with 10 mM $Ca^{2+}$. All external solutions were adjusted to pH 7.2 and 300–320 mosmole/Kg. All experiments were carried out at room temperature (~20°C).

Patch electrodes were pulled from Corning 7052 glass (Warner Instruments, Hamden, CT) and had resistances of 1–3 MΩ. Whole-cell capacitance, calculated as the area under a linear capacitive transient elicited by a −10 mV pulse, was 6–25 pF. Series resistance, calculated from the capacitive transient, was between 5 and 13 MΩ. The charging time constant was typically 100 μs. The linear capacitance was analogically subtracted as described in Shirokov et al. (1998), unless stated otherwise. Parameters of the compensation circuitry were set with a 20 mV pulse from −90 mV to reduce residual linear transients. The capacitive transients thus recorded are gating currents. Occasionally, as a reference, asymmetric currents were obtained after subtraction of scaled control currents and compared with those obtained with the analogic subtraction procedure. In these cases, control currents were elicited by pulses from −90 to −110 mV, before each depolarization and after holding the cell at −90 mV for 30 s.

Charge transfer was calculated as the time integral of the current transient after subtraction of a steady current, determined as the average over 10 ms at the end of the pulse. Data are presented as averages ± SE. Exponential time courses were fitted by the function $Y_1 = b + a\exp(-t/\tau)$ or the function $Y_2 = b + a_{slow}\exp(-t/\tau_{slow}) + a_{fast}\exp(-t/\tau_{fast})$. In all cases in which both fits converged, the statistical significance of the fit improvement provided by the two-exponential function $Y_2$ was evaluated. The test was based on the likelihood ratio statistic $LRS = (ssr_1 - ssr_2)/\sigma^2$ (Bickel and Doksum, 1977), in which $ssr_1$ and $ssr_2$ are the sums of squares of the residuals for the two fits, and $\sigma^2$ is the variance of the record. *LRS* has a $\chi^2$ distribution with 2 degrees of freedom (the difference between the number of free parameters of $Y_2$ and $Y_1$). If the statistic exceeds 6.0, the improvement in fit provided by the two-exponential function is significant, to >5%. $\sigma^2$ was estimated by $ssr_2/(N-5)$, which, being probably in excess, gave an underestimate of *LRS*.

## RESULTS

### Gating currents inactivate in two kinetic stages

Current methods for the study of VDI of cardiac L-type $Ca^{2+}$ channels use $I_{Ba}$ (Kass and Sanguinetti, 1984; McDonald et al., 1994; Hering et al., 2000). Because there is $Ba^{2+}$-dependent inactivation (Markwardt and Nilius, 1988; Mazzanti et al., 1991; Ferreira et al., 1997b), VDI is defined here as that which affects the voltage sensor, and is evaluated through the effects on intramembranous charge movements.

As with the dihydropyridine (DHP) receptor of skeletal muscle and voltage-dependent $Na^+$ and $K^+$ channels, there is a shift of the *Q-V* curve to more negative voltages upon inactivation of cardiac L-type $Ca^{2+}$ channels, native or heterologously expressed (Bezanilla et al., 1982; Starkus and Rayner, 1991; Bezanilla, 2000; Shirokov et al., 1992; 1998; Josephson, 1996). The time course of such shift upon conditioning depolarizations of different durations was studied as a measure of the onset of VDI. Fig. 1 shows the result of such an experiment in a typical cell expressing the $Ca_v1.2$ channel. To obtain the *Q-V* curve, test pulses in the range of −170 to 90 mV were applied from a brief 50-ms interpulse at −60 mV, where charge movement activation starts (Fig. 1 *A*). As detailed in Methods, the transient portion of the capacitance-compensated record is largely constituted by gating current. To inactivate the channel, conditioning

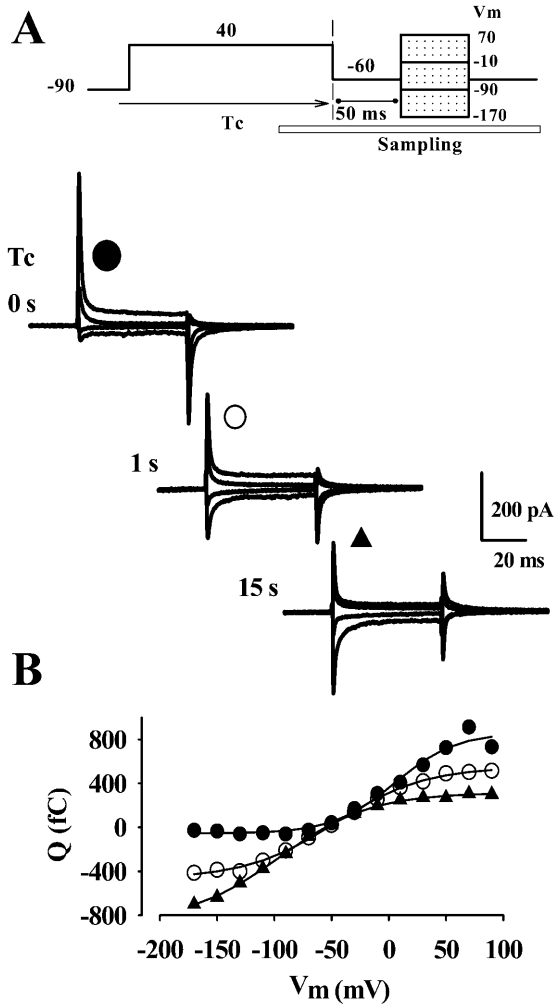


FIGURE 1 Voltage-shift of the gating charge upon inactivation. (*A*) Gating currents elicited by a test pulse (*protocol* at *top*) between an interpulse level of −60 mV and a variable test voltage, after an inactivating conditioning depolarization of duration $T_C$ to +40 mV. The three groups of currents correspond to different $T_C$, as indicated. (*B*) Charge transfer versus test voltage, obtained from the records shown in *A*. (●), $T_C = 0$ s (*reference*); (○), $T_C = 1$ s; and (▲), $T_C = 15$ s. Curves are fits of the function $Q = Q_T/(1 + \exp-(V_m - V_{1/2})/K) - Qn$. Values for this cell were: $Q_T = 1000 f_C$ for all conditioning durations, $V_{1/2} = 4.95$ mV ($T_C = 0$ s), −47 mV (for $T_C = 1$ s), and −70 mV (15 s). $K = 27$ mV (0 s), 35 mV (1 s), and 37 mV (15 s).

depolarizations to +40 mV of increasing durations (listed as $T_C$ in Fig. 1) were applied before the test pulses (Fig. 1 *A*). In the absence of inactivation ($T_C = 0$ s), most of the charge moves at potentials positive to −60 mV (Fig.1 *B*). Upon a 1-s conditioning depolarization there is a reduction in the amount of charge that moves positive to −60 mV and an increase in the amount of charge that moves negative to −60 mV. *Qp*, the charge moved by a large positive pulse from −60 mV, measures approximately the amount of charge available for channel activation (Charge 1), while *Qn*, transferred during a large negative pulse from the same starting voltage, measures the charge available to move in

inactivated channels (Charge 2; see Shirokov et al., 1992, 1998). Unless stated otherwise, *Qn* and *Qp* are measured at the leading edge of the test pulse. According to the *Q-V* plots in Fig. 1 *B*, the reduction in *Qp* caused by inactivating pulses equals the increment in *Qn*. The magnitude of such complementary changes increased with $T_C$, reaching asymptotically a maximum at ~15 s. For each conditioning duration, the dependence of the charge transfer on the membrane potential ($V_m$) was well-fitted by the Boltzmann expression

$$Q(V_m) + Qn = Q_T/\{1 + \exp[-(V_m - V_{1/2})/K]\}, \quad (1)$$

where $Q(V_m)$ is the charge moved upon depolarization from −60 mV to $V_m$; $V_{1/2}$ is the potential of equi-distribution; *K* a steepness parameter; and $Q_T$ the expression's maximum. Thus, upon inactivation, the total charge ($Q_T$) is conserved and the slope factor (*K*) is increased (value range 27–37 mV).

*Q-V* curves, averaged after normalization by $Q_T$, are shown in Fig. 2 *A* for conditioning depolarizations of increasing duration. The solid lines represent the best fits by Eq. 1 (without *Qn*). Inactivating conditioning pulses of longer duration caused a greater voltage shift. $V_{1/2}$ is plotted versus $T_c$ in Fig. 2 *B*. The inset shows that $V_{1/2}$ evolves as the sum of two exponentials, of time constants 0.5 s and 4 s, with the fast component comprising 60% of the total. The best fit of a single exponential plus a constant (equation for $Y_1$ as described in Methods; see also Fig. 2, *dashed line*), does not well-describe the data. Therefore, viewed through the resulting shift in the voltage distribution of the mobile charge, onset of VDI proceeds with two distinct kinetic components.

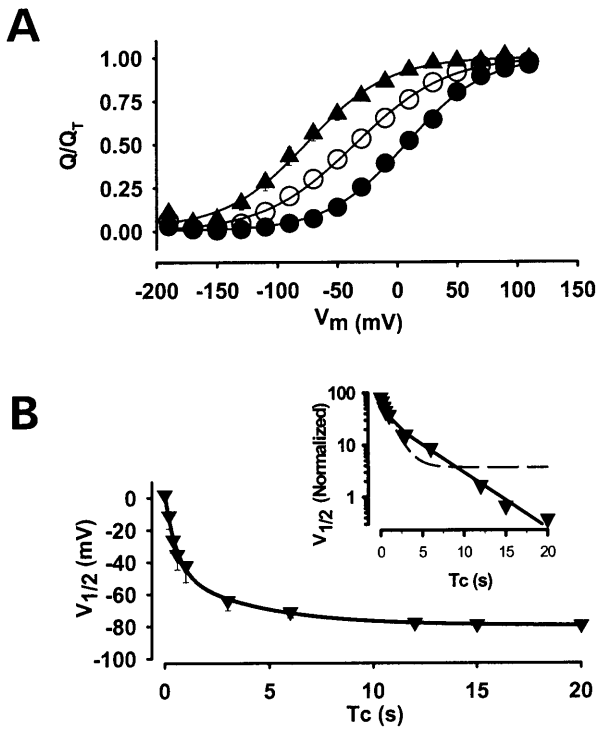


FIGURE 2 The shift in $V_{1/2}$ evolves with two kinetic components. (*A*) Average *Q* versus *V* in 12 experiments with the protocol illustrated in Fig. 1. Before averaging, charge transfer was shifted to a value of '0' at large negative voltages, and normalized to its maximum, $Q_T$, in the same experiment. (●), $T_C = 0$; (○), $T_C = 1$ s; and (▲), $T_C = 15$ s. Curves represent the best fit of the function $1 / (1 + \exp-(V_m - V_{1/2})/K)$ to each set. (*B*) $V_{1/2}$ versus $T_C$. The curve represents the best fit with the function $V_m = V_{1/2\ fast} \exp(-t/\tau_{fast}) + V_{1/2\ slow} \exp(-t/\tau_{slow}) + V_{1/2\ inf}$. Best fit parameters of the double exponential fit were: $V_{1/2\ fast} = 48 \pm 8$ mV; $\tau_{fast} = 0.52 \pm 0.07$ s $V_{1/2\ slow} = 36 \pm 8$ mV; $\tau_{slow} = 4.15 \pm 2.05$ s; and $V_{1/2\ inf} = -79.05$ mV. For the semilog plot, $V_{1/2\ fast}$ and $V_{1/2\ slow}$ were normalized to the total change in $V_{1/2}$ ($\Delta V_{1/2,\ T} = V_{1/2,\ (TC,\ 0)} - V_{1/2\ inf}$). The dashed line represents the best fit of a single exponential plus a constant.

The same conclusion is reached studying the time courses of *Qp* or *Qn* moved at extreme test voltages during the onset of inactivation. In Fig. 3 *A* the values of charge transfer are plotted against test potential for a reference situation (''0 s conditioning'') and after two conditioning pulses of different duration (1 s and 15 s). The symbols corresponding to the extreme values of $V_m$, representing charges *Qp* or *Qn*, are enclosed within boxes in thick line, while boxes in thin line enclose charges elicited by intermediate test pulses, positive or negative. In Fig. 3 *B* are the boxed values, plus other values not shown in Fig. 3 *A*, plotted as a function of $T_C$. The evolution of *Qn* and *Qp* (*large symbols*) was similar, essentially parallel to the evolution of $V_{1/2}$ shown in Fig. 2 *B*. In contrast, the charge transfer at membrane potentials that did not elicit maximal charge movement (*small symbols*) was not very dependent on $T_C$. Hence, it was of little use as a monitor of onset of VDI.

The increase in *Qn* and the reduction in *Qp* were normalized to the corresponding maximum values in every cell. Average normalized values are jointly plotted versus $T_C$ in Fig. 3 *C*. To better illustrate both components simultaneously, values were plotted on log scales. The solid lines represent the best fit by sums of two exponential functions. The kinetics of reduction of *Qp* mirror that of increase in *Qn*, as confirmed by the constancy of their sum (*dotted line* in Fig. 3 *C*), indicating the conservation of total mobile charge. To show at a glance the biexponential onset of VDI, the evolution of both types of charge versus conditioning duration was plotted in Fig. 3 *D* in a semilog scale. The dashed line represents the best fit of a single exponential plus a constant to the increase in *Qn*. The two-exponential fit (*solid line*) is clearly better. In agreement, the *LRS* was also high (~135), indicating significant improvement over the single exponential fit. For the evolution of *Qp*, the two-exponential fit was also justified compared with the single exponential (*LRS* ~ 27).

Measuring the onset of VDI through the increase in *Qn* has some advantages that will be used later in this article: 1), it provides information about the shift of the *Q-V* curve, from charge transfer data obtained at just one potential; and 2), it does not require blocking ions or drugs, as no ion channels are gated open at the required negative potentials, as argued before by Shirokov et al. (1993). The later advantage was used to measure onset of VDI in $Li^+$.

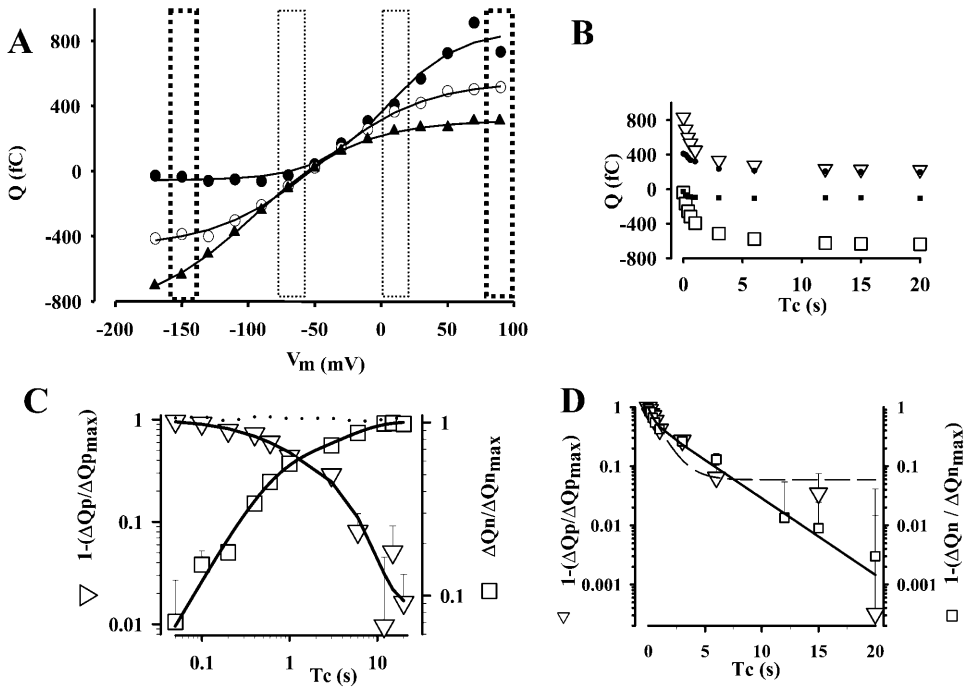


FIGURE 3 Charge transferred by large pulses varies with conditioning duration. (*A*) $Q$ versus $V$. The boxes mark test voltages for which the charge displacement will be represented versus $T_C$ in other panels. Boxes in thick dashed lines correspond to extreme voltages, eliciting $Qp$ or $Qn$.(*B*) Charge transferred at test voltages boxed, versus conditioning duration. For $Qp$ or $Qn$ the dependences with $T_C$ were close to a sum of two exponentials, and had a similar time course. At intermediate test voltages the changes in charge transfer were minor (*small black squares*). (*C*) Average change of $Qn$ or $Qp$ versus $T_C$ ($n = 14$), normalized and shifted as indicated to facilitate comparison. The best fit of a sum of two exponentials (*continuous line*), is superimposed. Addition of $Qp$ and $Qn$ is constant and is also shown in the same graph (*dotted line*). Log scales are used. (*D*) Semilog plots of data and fits of double and single exponential plus a constant (*continuous* and *dashed lines*, respectively). Coexponential promotion of $Qn$ was transformed in a exponential decay ($1 - \Delta Qn / \Delta Qn_{max}$). Best fit parameters: $Qn_{fast} = 0.51 \pm 0.03$, $\tau_{fast} = 0.47$ s $\pm$ 0.042, $Qn_{slow} = 0.49 \pm 0.03$, and $\tau_{slow} = 4.61$ s $\pm$ 0.834. $Qp_{fast} = 0.48 \pm 0.07$, $\tau_{fast} = 0.42 \pm 0.06$ s, $Qp_{slow} = 0.51 \pm 0.07$, and $\tau_{slow} = 3.8 \pm 0.8$ s.

In sum, inactivating depolarization determines a shift in the voltage distribution of mobile charge measured from an interpulse potential of −60 mV. The shift follows a biexponential time course, suggesting the existence of two processes. The time constants and relative amplitudes of the fast and slow components were the same when estimated with three different protocols (change in $Qn$, change in $Qp$, and evolution of $V_{1/2}$), reflecting the essential equivalence of all methods.

## The kinetic components remain separate during recovery

Recovery from VDI was evaluated measuring $Qn$ after a large inactivating depolarization and an interval of recovery of variable duration (*Tip*), as illustrated in Fig. 4 *A*. Fig. 4, *B* and *C*, shows plot currents, and Fig. 4 *D* shows charge transfers, in the leading edge of the large negative pulse that mobilizes $Qn$. After 1-s depolarizations, which mainly cause fast VDI, recovery of $Qn$ at −60 mV was almost complete in 4 s. Fig. 4 *E* shows that recovery from VDI is also well-described by the sum of two exponential functions, with time constants 0.17 s and 3.7 s. For this conditioning pulse, the relative amplitudes ($a_{fast} / (a_{fast} + a_{slow})$ and $a_{slow} / (a_{fast} + a_{slow})$) of the fast and slow recovery terms were 74% and 22%, respectively. Upon 20-s conditioning depolarizations (Fig. 4 *C*, and *large black symbols* in Fig. 4, *D* and *E*), recovery was also well-described by two exponentials of similar time constants, but the relative amplitudes of the components were 55% and 40%, respectively. Clearly, when a greater development of the inactivation of slow onset was allowed, the component of slow recovery increased as well.

To further examine this point, the amplitudes of each component of onset were compared with those of recovery in several cells. The amplitudes were normalized to $Q_T$ in each cell, to reduce variations in amplitude resulting from different expression levels, then plotted as onset versus recovery (Fig. 5). For both components, there was a strong correlation between amplitudes of onset and recovery. This finding suggests that inactivation proceeds along two alternative pathways of different kinetics—a dual view of inactivation, pursued further in the Discussion.

## Gating currents evolve with two known signatures

The kinetic separation of two components, which remains patent throughout onset and recovery, may correspond to two different inactivation mechanisms that, viewed through gating currents, might have signatures of charge immobilization or charge interconversion. Though both types of inactivation promote a reduction of charge related to activation, kinetics and voltage-dependence of recovery from inactivation are different. One of the signal features of charge immobilization is that the process of recovery is essentially cotemporal with the restoration of gating charge. Because such recovery becomes faster at more negative potentials, it is possible to monitor the return of gating charge

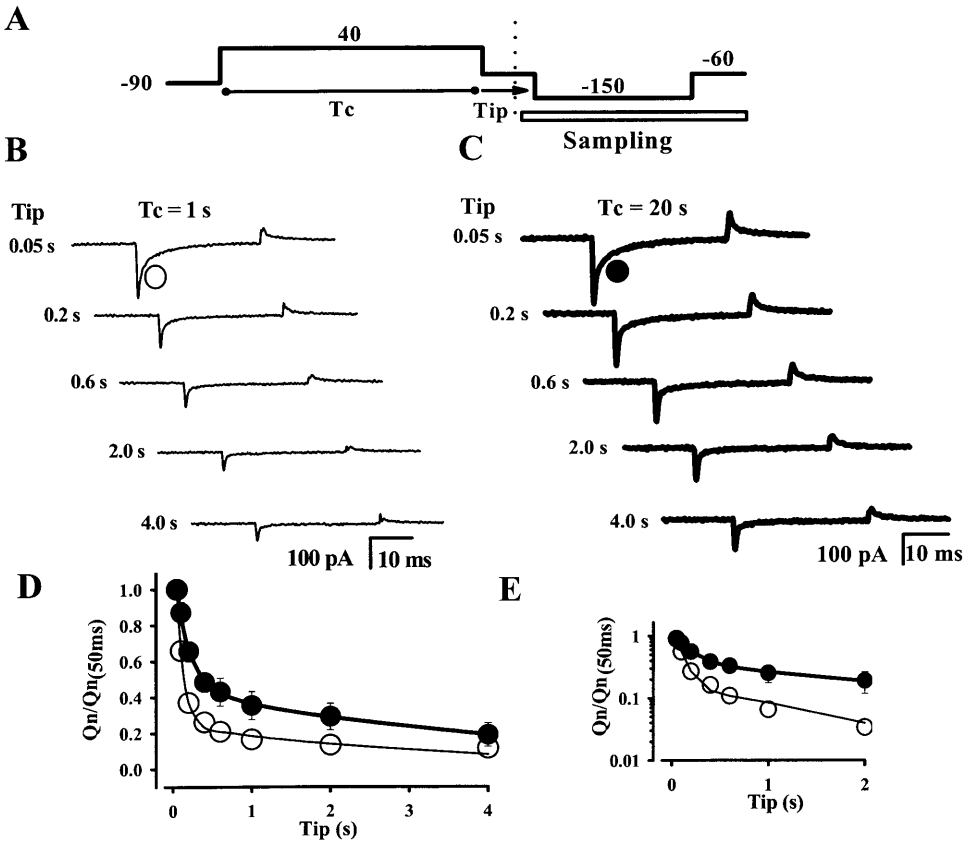


FIGURE 4 Recovery from VDI is described by two kinetically distinct components. Pulse protocol (*A*) and gating currents after 1 s (*B, left*) and 20 s (*C*, *right*) conditioning pulses and different recovery times (*Tip*, listed next to gating currents) at −60 mV. *Qn* diminishes as recovery time increases. (*D*) Average *Qn* (normalized to *Qn* after 50 ms of recovery) versus recovery time at −60 mV after $T_C = 1$ s ($n = 13$) or 20 s ($n = 8$). The slow component of recovery is increased upon a longer conditioning pulse. These results suggest that VDI that occurs slowly recovers slowly. (*E*) The semilog plot is shown. Best fit parameters for recovery of *Qn* after either conditioning pulse: $\tau_{fast} = 0.17$ s and $\tau_{slow} = 3.7$ s. Relative amplitudes: for $T_C = 1$ s, $a_{fast} / a_T = 0.74$, $a_{slow} / a_T = 0.22$; and for $T_C = 20$ s, $a_{fast} / a_T = 0.55$, $a_{slow} / a_T = 0.40$ ($a_T = a_{fast} + a_{slow}$).

from its immobilized state as a visible inward transient upon large hyperpolarizations. After returning to the *cis* position, this restored charge has all the usual properties, including its characteristic voltage-dependence activating in a range positive to −60 mV.

In contrast, the signature of charge interconversion is the appearance of a different mode of charge, which can move in either direction while the channel remains inactivated (Bezanilla et al., 1982; Brum and Rios, 1987; Starkus and Rayner, 1991). In this case, the charge is never immobilized but just voltage-shifted, mobile between its *cis* and *trans* positions with a $V_{1/2}$ near −90 mV (Shirokov et al., 1998). Because of these differences, it is possible to distinguish charge immobilization from charge interconversion by evaluating the ratio between transfers of charge at the *ON* (or leading) and *OFF* (or trailing) edges of a large negative-going pulse. For pulse durations shorter than the characteristic recovery times, an *ON/OFF* ratio much greater than '1' is expected for charge immobilization, while for charge interconversion the ratio should be near '1'. A more detailed justification of this prediction is given in the Discussion.

Test pulses to −150 mV were applied from an interpulse level of −60 mV (sustained for 50 ms), after different intervals $T_C$ of conditioning depolarization. Gating current traces are shown in Fig. 6 *A*. For every conditioning duration, the charge transfer was greater during the *ON* transient. The

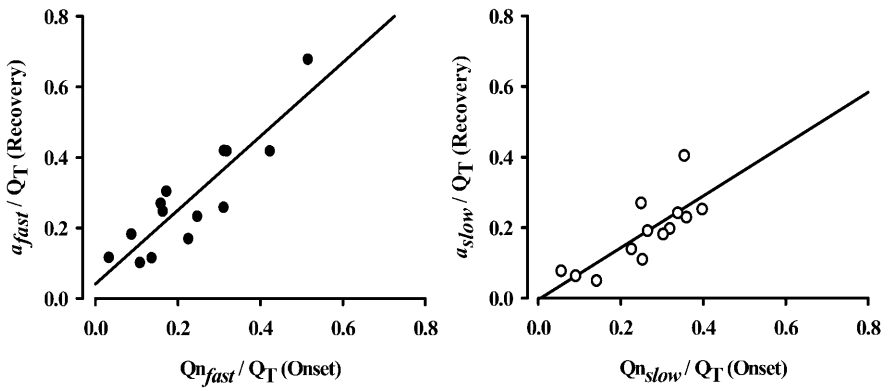


FIGURE 5 The amplitudes of kinetically distinct components of onset and recovery are highly correlated. (*Left*) Amplitude of fast recovery ($a_{fast}$) versus that of fast onset VDI ($Qn_{fast}$), normalized to $Q_T$ ($r^2 \sim 0.88$). (*Right*) Normalized amplitudes of slow recovery ($a_{slow}$) versus that of slow onset VDI ($Qn_{slow}$) ($r^2 \sim 0.81$). Amplitudes of both components were taken from each cell under experiments like those reported in Fig. 3 (*onset*) and Fig. 4 (*recovery*).

plot of the ratio (termed $Qn_{ON}/Qn_{OFF}$) versus $T_C$ is in Fig. 6 *B*. The ratio first increased with $T_C$, decreasing later to a steady level.

For conditioning of short durations, the proportion of fast VDI is greater, then decays at longer durations of conditioning, while that of slow inactivation increases. Hence the evolution of $Qn_{ON}/Qn_{OFF}$ when conditioning time increases is parallel to the relative weight of fast inactivation. In other words, when fast inactivation predominates, the *ON* and *OFF* transfers of *Qn* are very different. As argued before, this corresponds to the signature of charge immobilization (charge recovers rapidly to the resting state at −150 mV, producing the measurable *ON* transient, but this charge has normal voltage distribution; hence, it does not move in the *OFF* step to −60 mV.)

With the conditioning pulse of long duration, instead, the fraction of slow inactivation increases, and $Qn_{ON}/Qn_{OFF}$ was found to increase in parallel. This is consistent with conversion to Charge 2, which is distributed with a $V_{1/2}$ near −90 mV. Hence, it moves back and forth when $V_m$ is changed between −60 and −150 mV.

In conclusion, the changes in gating currents brought about by VDI were first found to take place in two kinetic stages, separate for both onset and recovery. They also present, separately in each kinetic component, the respective hallmarks of charge immobilization and charge interconversion, which in turn resemble features described for fast and slow inactivation in other voltage-dependent channels. Additional correspondences were found studying the voltage-dependence of recovery from inactivation.

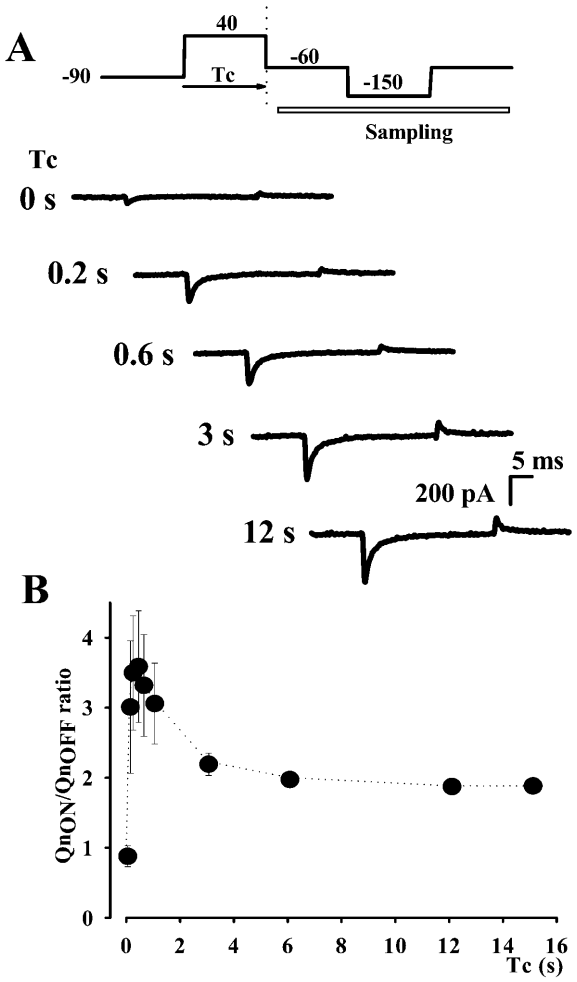


FIGURE 6 *Qn* induced upon fast and slow VDI has different signatures. (*A*) Records elicited by hyperpolarizing pulses, to obtain *Qn*. Longer-lasting conditioning depolarizations increased charge transfer in *ON* and *OFF* transients. $Qn_{ON}$ increases more and more rapidly than $Qn_{OFF}$. (*B*) $Qn_{ON}/Qn_{OFF}$ ratio for conditioning pulses of increasing durations ($n = 14$).

## Recovery from fast VDI is more steeply voltage-dependent than recovery from slow VDI

Voltage-dependence of recovery from fast VDI was studied determining the kinetics of reduction of *Qn* at a variable recovery or interpulse voltage, *Vip*, in a cell conditioned by a brief pulse at +40 mV (Fig. 7 *A*). Fig. 7 *B* shows traces of gating currents elicited by pulses from −60 to −150 mV, after different recovery times (*Tip* = 0.05 s or 0.1 s) and voltages (*Vip* = −60 or −120 mV). In Fig. 7 *C* are plots of average *Qn* (normalized to $Q_T$) versus recovery time at three values of *Vip*. It can be seen that recovery from fast inactivation was much faster at −120 mV than at −60 mV. The results additionally show that a 0.4-s sojourn at −120 mV is sufficient to recover from fast VDI. This observation suggests a method to evaluate the properties of slow VDI in isolation.

To study the voltage-dependence of recovery from slow inactivation, the duration of the conditioning pulse was increased to 12 s (Fig. 8 *A*) and the kinetics of recovery were determined at different voltages, as done previously. Additionally, slow VDI was isolated by preceding the variable interpulse by a fixed 0.4-s interval at −120 mV, which recovers the channels from fast VDI. Fig. 8 *B* shows gating currents, with *Tip* and *Vip* indicated next to the traces. The values of *Qn* thus obtained are plotted versus *Tip* and *Vip* in Fig. 8 *C*. There is little voltage-dependence of recovery. Recovery time constants, from single-exponential fits to data in Figs. 7 *C* and 8 *C*, are plotted versus *Vip* in Fig. 8 *D*. The voltage-dependence of recovery from fast VDI (*open symbols*) is steeper than that of slow VDI.

## A slow phase of charge movement increases during fast VDI

A characteristic feature in the onset of charge immobilization is the appearance of a relatively slow phase of gating current decay during the *OFF* of a depolarizing pulse. This slow component has the time course of recovery from inactivation and part of it is lost in the baseline noise at repolarizing potentials (−70 mV). The charge movement underlying that

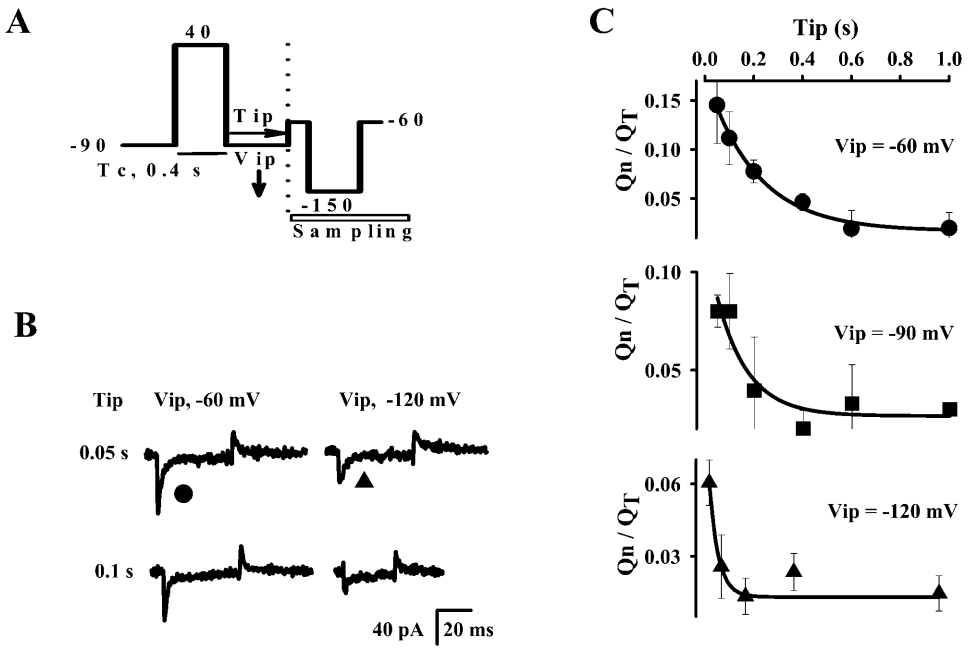


FIGURE 7 Voltage-dependence of recovery from fast VDI. (*A*) Pulse protocol: a 0.4-s conditioning pulse promotes fast VDI with negligible slow VDI. (*B*) Representative gating currents for recovery times (*Tip*) and voltages (*Vip*) indicated. *Qn* was recorded between −60 and −150 mV. (*C*) Average values of recovery of *Qn* normalized to $Q_T$, at different recovery voltages ($n = 6$). The time constants corresponding to *Vip* −60, −90, and −120 mV, were 0.2, 0.12, and 0.037 s, respectively.

phase, increases its relative weight in $Q_{OFF}$ with the onset of inactivation (Armstrong and Bezanilla, 1977). As inactivation develops, charge movement in the *OFF* fast phase diminishes whereas that in the *OFF* slow phase increases. Seeking such features, the *OFF* kinetics of the gating currents were studied with the pulse protocol in Fig. 9 *A*: pulses of different durations to +40 mV, followed by repolarization to −60 mV. *OFF* gating current was adequately fitted by the sum of two exponentials, of which the slow one is represented in Fig. 9 *B*. With longer lasting depolarizations, the gating charge transferred in the *OFF* was reduced, while the relative weight of gating charge associated with the slow phase was increased. The amount of charge transferred by each phase is plotted versus pulse duration in Fig. 9 *C*. The complementary changes in magnitude are associated with fast VDI, as both develop in a similar time range of less than 1 s.

Together, these properties of fast VDI resemble charge immobilization in voltage-dependent $Na^+$ and $K^+$ channels (Armstrong and Bezanilla, 1977; Roux et al., 1998). The sole difference is in the timescales of onset, which in the $Ca^{2+}$ channel are at least tenfold slower.

## Fast VDI is modulated by extracellular cations

When divalent ions are removed from the extracellular solutions, $Ca^{2+}$ channels become permeant to monovalent cations (Hess et al., 1986). Two prior observations—that the kinetics of inactivation of L-type $Ca^{2+}$ channel currents carried by monovalent ions is slow in native and expressed channels (Hadley and Hume, 1987; Ferreira et al., 1997b), and that mutations in the IS6 region (presumably a part of the channel pore) alter VDI substantially (Zhang et al., 1994)—suggest that divalent ions may play a role in fast VDI. This possibility was tested in measurements with $Li^+$ as the main extracellular cation.

Inactivation of $Li^+$ current through the expressed $Ca^{2+}$ channels is very slow (Fig. 10 *A*). We determined the onset of VDI in these conditions ($Li^+$ substituted for $Ca^{2+}$) measuring *Qn* after conditioning depolarizations of increasing durations (Fig. 10 *B*), at conditioning voltages shifted by approximately −40 mV to offset the electrostatic changes in the absence of divalent ions. Gating currents, in Fig. 10 *C*, show that *Qn* did not increase rapidly with conditioning duration, and that $Qn_{ON}$ and $Qn_{OFF}$ were nearly equal. Linear capacitive transients were not greatly affected by extracellular substitution of $Li^+$ for $Ca^{2+}$. However, the time course of the gating currents corresponding to *Qn* was slower than that obtained in solutions with di- or trivalent cations. This finding suggests that remotion of di- or trivalents from the extracellular solution unmasks (or leads to) slow voltage-dependent steps. The plots of charge transfer versus $T_C$ (log scales in Fig. 10 *D*, and semilogarithmically in Fig. 10 *E*) are well-fitted by a single exponential (*LRS* = −0.91). This is in clear contrast with the onset of *Qn* in the presence of $Ca^{2+}$ and $Gd^{3+}$, whose fit, reproduced from Fig. 3 *C*, is represented by the thin dashed line. Onset of inactivation also followed a double exponential in extracellular solutions containing 10 mM $Ca^{2+}$ or $Ba^{2+}$ without $Gd^{3+}$, or $Gd^{3+}$ alone (data not shown). These results imply that fast VDI is virtually absent in $Li^+$ extracellular solution. What remains is a slow inactivation, with similar kinetics to slow VDI. In conclusion, fast VDI requires the presence of divalent (or trivalent) ions in the extracellular solution, while the slow inactivation does not.

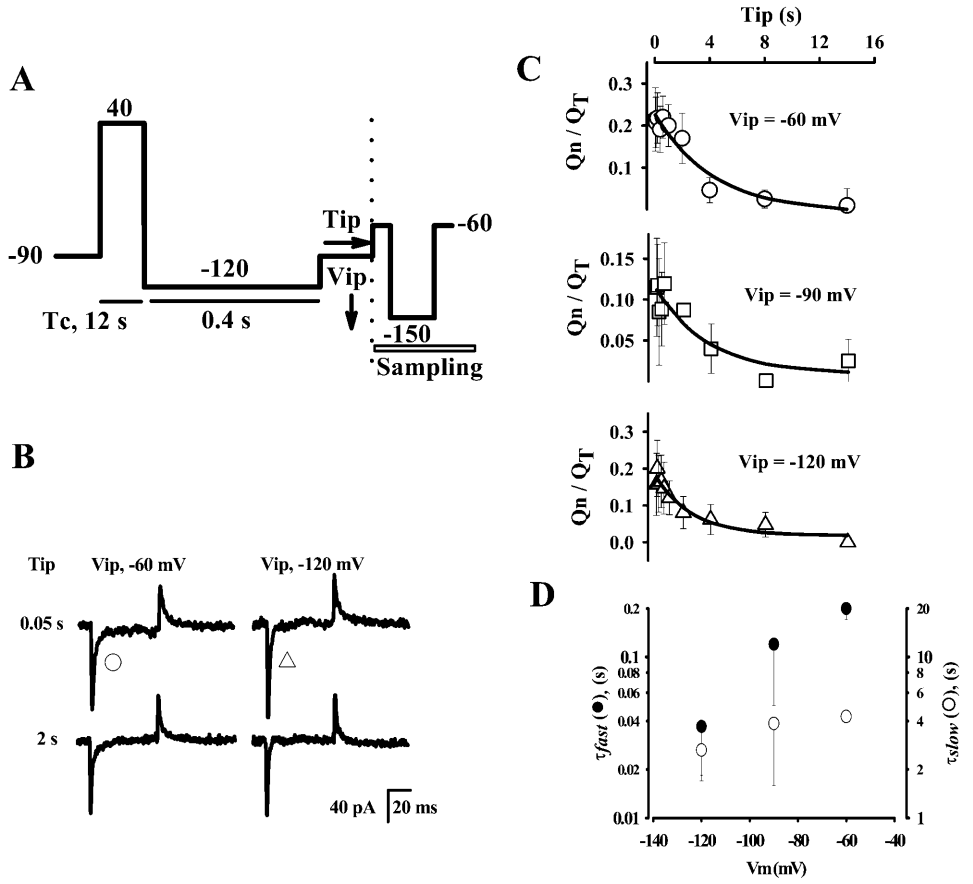


FIGURE 8 Voltage-dependence of recovery from slow VDI. (*A*). Protocol: a 12-s conditioning pulse (of duration sufficient to induce slow VDI), followed by a 400-ms interpulse to −120 mV (to allow recovery from fast VDI). (*B*) Representative gating currents for recovery times (*Tip*) and voltages (*Vip*) indicated. (*C*) Average values of recovery of *Qn* normalized to $Q_T$, at different recovery voltages ($n = 5$). (*D*) Semilog plot of time constants of recovery ($\tau_n$) versus recovery voltages. For better comparison, the maximum changes in scales for the right and left axis are of the same order of magnitude. Time constants were obtained from the best single exponential fits to plots shown in Figs. 7 *C* and 8 *C*. Values for *Vip* −60, −90, and −120 mV, were 4.2, 3.8, and 2.7 s, respectively. Voltage-dependence of recovery from fast VDI is steeper than that of slow VDI.

## DISCUSSION

Inactivation of cardiac L-type $Ca^{2+}$ currents may be caused by the permeant ions, the applied change in transmembrane potential, or both. In previous work, we and others have shown that these influences are separate, with voltage effects occurring regardless of, and independent from, the ionic current (Shirokov et al., 1993; see also Hadley and Lederer, 1991). This separation has given rise to a popular paradigm for isolation of VDI, the substitution of $Ba^{2+}$ for $Ca^{2+}$. However, $Ba^{2+}$ going through the channel is capable of inducing a degree of (ion or current-dependent) inactivation (Markwardt and Nilius, 1988; Mazzanti et al., 1991; Ferreira et al. 1997b). Additionally, Shirokov (1999) demonstrated further entanglement of voltage- and ion-dependent inactivation in N-type $Ca^{2+}$ channels. Hence, there is no completely satisfactory method to isolate VDI of ionic currents without some kind of ionic manipulation that will affect inactivation.

To solve the conundrum, in the present work VDI was examined largely through its effects on the voltage sensor, as monitored by intramembranous charge movement. The consequences of VDI at the level of charge movements consist of a number of changes with two main outcomes: First, an inactivation of gating charge which progressively disappears, i.e., ceases to be mobile in the voltage range where it is normally activated; second, charge movements become increasingly prominent in a voltage range negative to the resting potential (more specifically, negative to a ''watershed'' potential near −60 mV). Thus, two reciprocal changes in charge movement accompany VDI, a decrease in charge transferred at potentials positive to −60 mV (termed *Qp*) and an increase in *Qn*, mobile upon hyperpolarization from −60 mV. The overall result can also be described as a negative shift of the *Q-V* distribution upon inactivation.

We examined these changes in L-type cardiac $Ca^{2+}$ channels expressed in tsA201 cells, which are virtually devoid of other voltage-dependent channels. The time course of the shift of the *Q-V* curve during the onset of inactivation was found to have two components. Although the kinetics of shift of the *Q-V* curve have not been studied in $Ca^{2+}$ channels before, some groups have proposed the existence of multiple VDI mechanisms based on the kinetics of inactivation of $Ba^{2+}$ currents in native cells (Kass and Sanguinetti, 1984; Kay, 1991; Boyett et al., 1994; Nilius et al., 1994; Cox and Dunlap, 1994) and more recently in expressed $Ca^{2+}$ channels (Hering et al., 2000; Stotz and Zamponi, 2001a). These studies had problems, due to the presence of multiple types of $Ca^{2+}$ channels in native cells and the existence of a $Ba^{2+}$-dependent inactivation (Markwardt and Nilius, 1988;

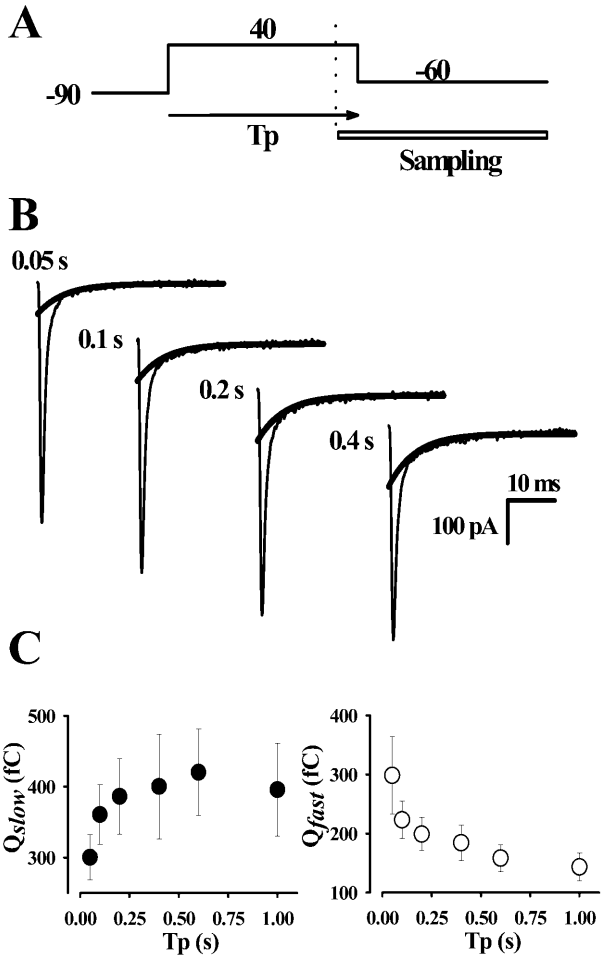


FIGURE 9 A slow phase of charge movement increases during the onset of fast VDI. (*A*). Pulse protocol: gating currents were recorded at the trailing edge of test pulses of different durations (*Tp*). Sampling rate was changed immediately before the end of the test pulse. (*B*) *OFF* gating currents after depolarizations of different durations (*listed*) in the time range of fast VDI. (*Thick trace*) Slow term of the two-exponential fit. (*C*). Average values of charge transferred by fast ($Q_{fast}$) and slow ($Q_{slow}$) terms of the fit ($n = 12$).

Mazzanti et al., 1991; Ferreira et al., 1997b), which obscures VDI processes. In contrast, monitoring VDI at the level of the voltage sensor does not have these problems, revealing unequivocally two distinct kinetic components in VDI. Several features of these components indicate that the duality is fundamental. One is that the kinetic separation remains patent upon recovery, indicating that the channels that inactivated slowly also recover slowly; these components correlated well with kinetic components in the recovery from inactivation, suggesting alternative pathways of inactivation. Second, there were clear differences in the voltage-dependence of recovery. Third, the fast component of inactivation appeared to have a strict requirement for the presence of divalent cations in the extracellular medium. A more detailed analysis of the changes in gating currents associated with both components confirmed the duality, while highlighting a rough similarity between the two components of

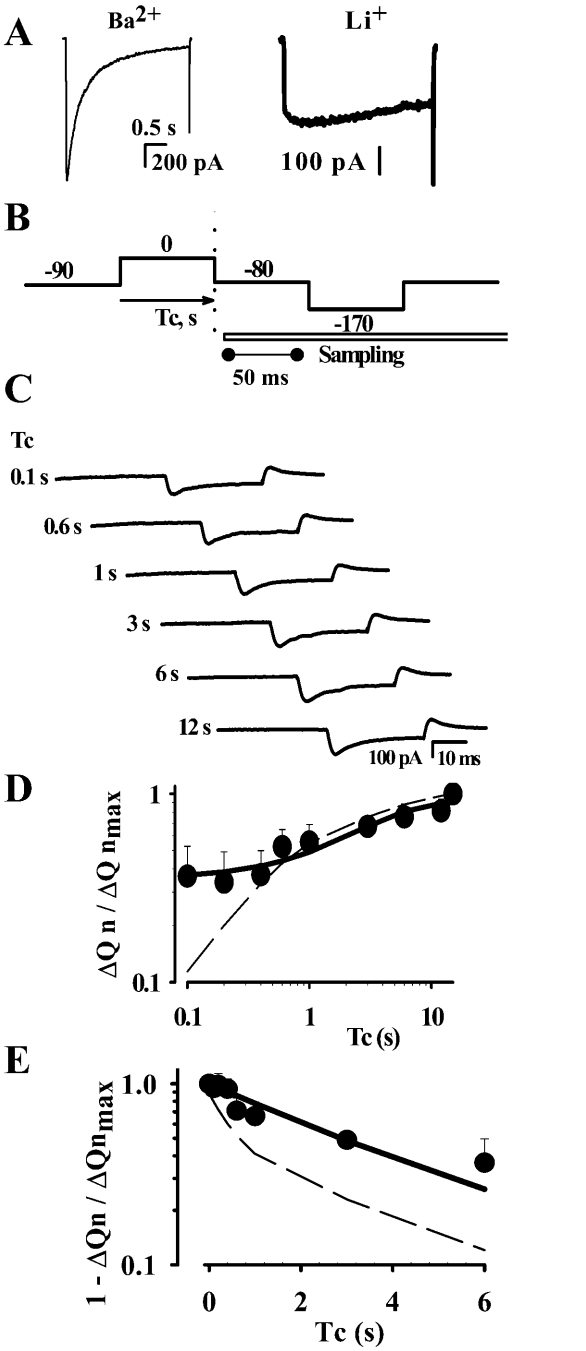


FIGURE 10 Onset of $Qn$ in $Li^+$ has a single kinetic phase. (*A*) Typical course of $Li^+$ and $Ba^{2+}$currents through expressed cardiac L-type $Ca^{2+}$ channels. Fast VDI is greatly diminished in $Li^+$. (*B*) Two-pulse protocol used to obtain $Qn$ in $Li^+$ solution. Voltages accounted for the 30 ~ 40 mV screening. (*C*) Gating currents in $Li^+$ solution, elicited by pulses to −170 mV (*D*) Onset of $Qn$ in $Li^+$ solution. Averages of $\Delta Qn$ / $\Delta Qn_{max}$ versus conditioning duration ($n = 6$) on log scales. (*Solid line*) Single exponential fit. (*Dashed line*) Two-exponential fit to data in $Ca^{2+}$-containing "charge" solution (from Fig. 3). The onset of $Qn$ in $Li^+$ solution is very similar to the slow component in $Ca^{2+}$-containing solution. (*E*) Semilog plot. Parameter values: $\tau = 3.6$ s, $a = 0.86$, and $b = 0.14$.

inactivation seen here and the fast and slow inactivation processes of other voltage-operated channels.

## Fast VDI entails charge immobilization and slow VDI charge interconversion

Charge immobilization and charge interconversion are caused by distinct effects of inactivation at the level of the voltage sensor, which in turn correspond to different structural underpinnings in the voltage-dependent channels in which they have been described.

''Immobilization'' of the gating charge during fast inactivation in voltage-dependent $Na^+$ and $K^+$ channels has several characteristics (Bezanilla, 2000): 1), reduction in the charge transferred in the *OFF* transient upon repolarization; 2), increase in a slow component of *OFF* charge movement; 3), steep increase in rate of recovery at large negative voltages; and 4), perhaps most crucially, recovery of the standard, noninactivated properties of the gating charge immediately upon return to the *cis* position. *Charge immobilization* is usually related to open channel block by a cytoplasmic tethered particle. This process is fast and slows the return of the voltage sensor to its resting position, resulting in the ''immobilization'' of charge (Yellen, 1998; Bezanilla, 2000). Recovery of this interference is quite voltage-dependent, leading to the loss or reduction of the shift of the *Q-V* curve for recovery times that outlast charge movement. This is especially well-seen at hyperpolarizing potentials. In other words, the movement of charge at hyperpolarizing potentials coincides with its repriming. As we show in this report, fast VDI in $Ca_v1.2$ features these biophysical characteristics, suggesting that it is caused by charge immobilization.

Meanwhile, *charge interconversion* (as described, for instance, in the inactivation of skeletal muscle $Ca^{2+}$ channels, and in the slow inactivation of $Na^+$ channels of the squid axon and *Shaker* $K^+$ channels) features mostly the first of the properties listed above. Particularly telling is the difference in the fourth property. The gating charge of a slow-inactivated channel may return to the *cis* position upon hyperpolarization, without recovery of its resting properties, including the ability to gate the channel (Bezanilla et al., 1982, Starkus and Rayner, 1991; Olcese et al., 1997). Such inactivated charge is termed Charge 2 in skeletal and cardiac L-type $Ca^{2+}$ channels (Brum and Rios, 1987; Shirokov et al., 1992, 1998). Thus, charge interconversion is consistent with a more stable change in the channel function upon inactivation. The process sets up slowly and is basically modal regarding the effects at the level of charge movement. It is seen mainly as a shift of the *Q-V* curve, maintained for recovery times that outlast charge movement, even upon hyperpolarization. In this case, the repriming of charge at hyperpolarizing potentials outlasts its own movement. The molecular mechanisms underlying the effects of slow inactivation in the gating charge are unknown and might be different among distinct voltage-dependent channels. So far, in voltage-dependent $Na^+$ and $K^+$ channels, it has been related to comprehensive changes in the channel molecule, involving the outer mouth and selectivity filter (Baukrowitz and Yellen, 1995; Loots and Isacoff, 1998; Yellen, 1998). The present findings regarding slow VDI are consistent with previous results in expressed $Ca_v1.2$ channels (Shirokov et al., 1998), which mainly regarded the steady-state properties of inactivation. They are also consistent with evidences of charge interconversion described also at the level of the cardiac L-type $Ca^{2+}$ native channel (Shirokov et al., 1992; Ferreira et al., 1997a; Josephson, 1996).

## A ring of four states accounts for either charge immobilization or charge interconversion

The properties of charge immobilization are roughly featured by a state model, represented in Diagram 1, in which the channel evolves among a resting (*C*), an open (*O*), and an inactivated state (*I*). Transitions $C \leftrightarrow O$ and $C \leftrightarrow I$ have voltage-dependence, which is not required for $O \leftrightarrow I$. However, models of this type do not reproduce fully several kinetic aspects of gating currents, which are better described by allosteric models of inactivation (Roux et al., 1998).

A minimum allosteric model that can reproduce both

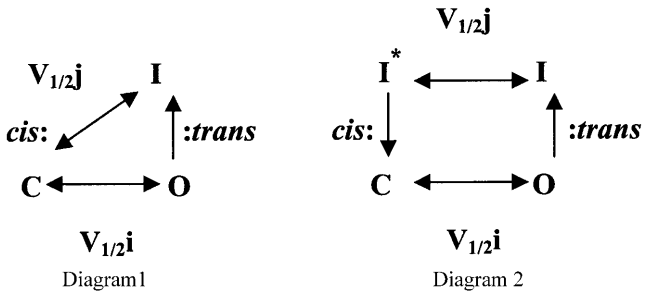


features of charge immobilization and charge interconversion has four states, and is represented in Diagram 2. As argued before by Shirokov et al. (1998), this minimal model can describe qualitatively different inactivation processes, according to the voltage-dependence and ratios between rate constants. The four-state model has the additional state *I** compared to Diagram 1. This state is inactivated closed, with the mobile charge in its *cis* position. In this minimal model inactivation is allosterically coupled to the movement of the activation gate. Extensions of this minimal model have been usefully applied to describe a variety of inactivation processes in several voltage-dependent channels (Marks and Jones, 1992; Kuo and Bean, 1994; Roux et al., 1998; Olcese et al., 1997).

In the ring of four states model, only the horizontal transitions are voltage-dependent. These transitions are fast and account for measurable charge movement. Vertical transitions are voltage-independent. Assuming that the intrinsic

microscopic rates of voltage-dependent steps are symmetric and have the same slope factor, the half-distribution potential among inactivated states ($V_{1/2}j$) is related to that of activation ($V_{1/2}i$) by the following equation,

$$V_{1/2}j = V_{1/2}i + K(\ln K_R/K_I), \quad (2)$$

where $K$ is the slope factor, and $K_I$ and $K_R$ are the equilibrium constants of the $O \leftrightarrow I$ and $C \leftrightarrow I^*$ transitions, respectively (Brum and Rios, 1987). If $K_R \ll K_I$, then $V_{1/2}j$ is more negative than $V_{1/2}i$ and, as a result, during inactivation, the *OFF* charge from an inactivating depolarizing pulse will be reduced.

If vertical transitions are slow compared to the voltage-dependent ones, the model describes charge interconversion. In this case, the speed of recovery is mostly limited by the transition $I^* \rightarrow C$, which is slow and voltage-independent. In a channel with these characteristics, the charge will return upon hyperpolarization; but recovery (of resting properties of gating charge and channel availability to open) requires the additional $I^* \rightarrow C$ step. As a result, recovery of charge does not show a steep voltage-dependence, and it outlasts its own movement—explaining experimental findings of charge interconversion (Shirokov et al., 1998). Hence, in charge interconversion, different modes of charge movement can be defined and determined experimentally. In inactivated channels, charge moves with a different $V_{1/2}$ and in the case of charge interconversion, this shift of the $Q$-$V$ curve toward more negative voltages is clearly observed regardless of the interpulse voltage. In skeletal and cardiac muscle L-type $Ca^{2+}$ channels, these modes of charge have been termed Charge 1 (moving between the states $C$ and $O$) and Charge 2 (moving between the inactivated states; see also Brum and Rios, 1987; Shirokov et al., 1992, 1998).

If vertical transitions are fast and have similar rates in the range of those exhibited by the horizontal voltage-dependent steps, then the model no longer shows a modal behavior of charge movement. As the $I^* \rightarrow C$ transition is fast, charge recovers mostly while it moves back to its *cis* position, and with hyperpolarizing voltages in the interpulse, a shift in the $Q$-$V$ curve is less well-defined. Under these circumstances, the rate of recovery is limited mostly by charge movement among inactivated states and the four-state model behaves similarly to the model depicted in Diagram 1. This leads to a steeper and faster voltage-dependence of recovery in comparison with charge interconversion. Taking this into account, charge immobilization may accordingly be viewed as a ''charge interconversion of fast recovery.'' These characteristics also feature the appearance of a slow component of charge movement in the *OFF* gating currents, as it is classically described in charge immobilization.

In sum, an allosteric four-state model with different sets of parameters (particularly the microscopic rates of the $I^* \leftrightarrow C$ transition) can give distinct qualitative behaviors describing either charge immobilization or charge interconversion.

The model is also useful to explain the differences, documented in Fig. 6, in the $Qn_{ON}/Qn_{OFF}$ ratio after fast or slow inactivation. In the case of *slow inactivation*, $Qn$, the charge that moves between −60 and −150 mV, is simply Charge 2. This is a well-behaved charge, moving rapidly between two stable states that do not recover significantly to $C$. Hence, equality between *ON* and *OFF* transfers is featured. After *fast inactivation*, the charge that moves in the *ON* transient of a hyperpolarizing pulse corresponds to the transition $I \leftrightarrow I^*$, but in this case it recovers rapidly to $C$ because the rate of $I^* \rightarrow C$ is fast. Therefore, the trailing edge of the hyperpolarizing pulse finds the charge in its resting (''remobilized'') state. As $V_{1/2}j$ is negative (~50 mV for fast VDI) and $V_{1/2}i$ is ~0 mV, $K_R$ should be low compared to $K_I$. As $K_R$ is equal to the ratio of the microscopic rates of transitions $C \rightarrow I^*$ and $I^* \rightarrow C$, the microscopic rate of $C \rightarrow I^*$ should be low. Because of these features, charge will not transition to $O$ at potentials below −60 mV explaining, in this way, the large asymmetry of $Qn_{ON}/Qn_{OFF}$ ratio during fast inactivation.

## A nine-state model of VDI

A nine-state model with two alternative pathways of inactivation accounts for most of the observations reported in this article (Fig. 11 *A*). The model does not seek to describe CDI. It is an extension of the minimal four-state model discussed before and depicted in Diagram 2. The channel activates in two steps to take into account closed states in the activation pathway as well as inactivation from closed states. Fast and slow parallel inactivation pathways diverge from the open state. Voltage-dependent transitions are represented horizontally. Vertical transitions leading to and from inactivated states are voltage-independent. The transition that represents fast VDI from the open state requires the presence of extracellular divalent cations.

With the parameter values given in Fig. 11, $Qn$ is accounted for as the charge moved between inactivated states, while the simulated $Qp$ moves in the activation pathway. After a conditioning depolarization, available $Qp$ is reduced by charge immobilization in the fast inactivation pathway and by charge interconversion in the slow inactivation pathway. As voltage-independent transitions of recovery from fast VDI are rapid, the upper left state in the fast inactivation pathway is negligibly populated, reducing the effective population of states related to fast VDI to I2a and I3a. This leads to rapid transition to the closed states upon hyperpolarization. These recovery transitions are rate-limited by the horizontal step, and in consequence, voltage-dependent. Hence, in this case, voltage-dependence of recovery is steep at hyperpolarizing recovery voltages. The existence of I1a (*upper left state* in the *fast inactivation pathway*), is suggested by a shallow voltage-dependence of recovery at intermediate voltages (ranged from −90 to −50 mV). The absence of such a state would lead to a ring of three states

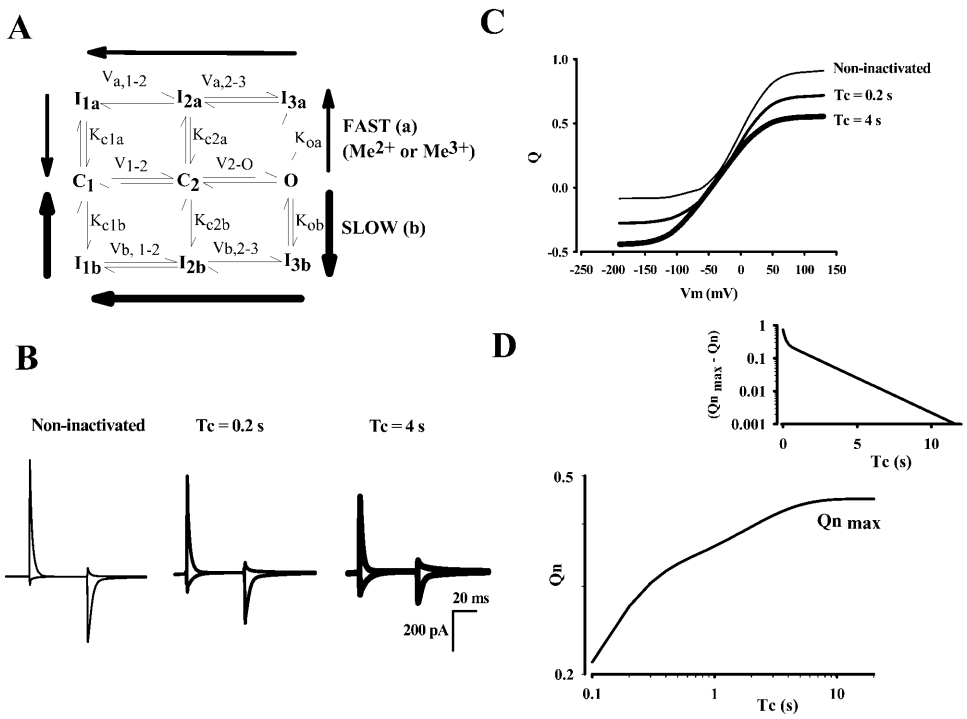


FIGURE 11 Simulations with a nine-state model. (*A*) Nine-state model with parallel inactivation pathways from the open state. Inactivation to state $I_j a$ is fast, and to state $I_j b$ is slow. Fast inactivation needs binding of di- or trivalent ions. Thick arrows indicate the preferred flow. Horizontal transitions are voltage-dependent. Vertical transitions are voltage-independent. $V_{1/2}$ were: for channel activation; $V_{1-2}$ = 0 mV, $V_{2-O}$ = 20 mV; for "fast inactivated" states, $Va_{1-2}$ = −50mV, $Va_{2-3}$ = −33 mV; for "slow inactivated" states, $Vb_{1-2}$ = −82 mV, $Vb_{2-3}$ = −67 mV. Values of $V_{1/2}$ for inactivated states in each ring were determined according to Eq. 2, once $V_{1/2}$ for related activation steps and vertical transitions constants were fixed. The slope factor, *K*, was set at 25 mV. Equilibrium constants to fast inactivation (*upper pathway*) are, from left to right (see *model*): 0.09, 0.7, and 6; to slow inactivation (*bottom pathway*) are, from left to right: 0.009, 0.247, and 8. Unidirectional kinetic constants to fast inactivation are (in $s^{-1}$), 8.9, 6.9, and 4; to slow inactivation, 0.015, 0.22, and 2.2. Intrinsic rate constants for voltage-dependent steps were assumed to be symmetric for forward and backward transitions. Values were, from top to bottom and left to right (in $s^{-1}$), 50, 30, 100, 170, 50, and 30. Microscopic reversibility was tested in each ring for each simulation. (*B*) Gating currents obtained with the model in a nonconditioning situation and after conditioning pulses to +40 mV of 0.2 s and 4 s. The holding potential was −90 mV. Traces shown were elicited by test pulses to −150 and +90 mV from a 50-ms interpulse to −60 mV. (*C*) Simulated *Q-V* curves. Despite the particular values of the conditioning pulses used for the simulation, the model reproduces well the observed reduction in *Qp* and increment in *Qn* with longer conditioning as reported in Fig. 1. (*D*) As in Fig. 3, onset of $Qn_{ON}$ follows a double-exponential time course. As in previous figures, log scales are used. The pulse protocol was similar to those in Figs. 3 *C* and 11 *B*, with a wider range of conditioning durations. Parameters obtained for the best fit of a sum of two exponentials were $\tau_{fast} = 0.13$ and $\tau_{slow} = 2.1$ s. Relative amplitudes were $a_{fast} / a_T = 0.60$ and $a_{slow} / a_T = 0.40$ ($a_T = a_{fast} + a_{slow}$). (*Inset*) Semilog plot.

like that shown in Diagram 1 (C1, C2, and I2a in the nine-state model). In such rings, a steep voltage-dependence of recovery is expected for all voltages below −50, provided that the $V_{1/2}$ of the $I \rightarrow C$ transition is similar to that found experimentally (−45 mV). By contrast, the intrinsically voltage-independent step of recovery from slow VDI is also the slowest. Hence, recovery from slow VDI will not feature a steep voltage-dependence. Slow VDI resembles inactivation of the DHP receptor of skeletal muscle, where two types of charge (Charge 1 and Charge 2) can be clearly distinguished, because of the slow rate-limiting steps of onset and recovery from inactivation.

The model describes several experimental findings. Simulated gating currents for extreme positive- and negative-going test pulses, are shown in Fig.11 *B*. Inactivation was induced by conditioning pulses to +40 mV, lasting 0.2 s (to elicit fast VDI) or 4 s (for slow VDI). These conditioning durations are approximately equal to the time constants of fast and slow VDI predicted with this set of parameters. Fig. 11 *C* plots charge transfer *Q* versus voltage, whereas the time-dependence of *Q* is represented in Fig. 11 *D* on log scales and semilogarithmically, to illustrate its evolution as sum of exponentials.

Simulations of recovery of gating currents after inactivation are illustrated in Fig. 12. Fig. 12 *A* represent recovery from fast inactivation, and Fig. 12 *B* the corresponding events after slow inactivation. The traces are gating currents elicited by a pulse to −150 mV from an interpulse at −60 mV with variable duration (*Tip*). Charge transfer (*Qn*) is plotted as a function of *Tip*. The time constants of onset and recovery from fast VDI are shorter in the model than in the data.

In sum, the model emulates well, qualitatively, most features of VDI: a negative shift of the *Q-V* distribution, onset and recovery after a sum of two exponentials, and different voltage-dependencies of recovery from fast and slow VDI.

## Structural implications for $Ca_v1.2$ channels

Several observations indicate that two different voltage-dependent inactivation mechanisms are at work in the cardiac L-type channel. For example, fast VDI depends on the nature of extracellular cations. When divalent cations were removed from the extracellular solution, to record the $Li^+$ currents through the channel, the fast component of VDI was greatly reduced (see Fig. 10). This finding suggests that fast

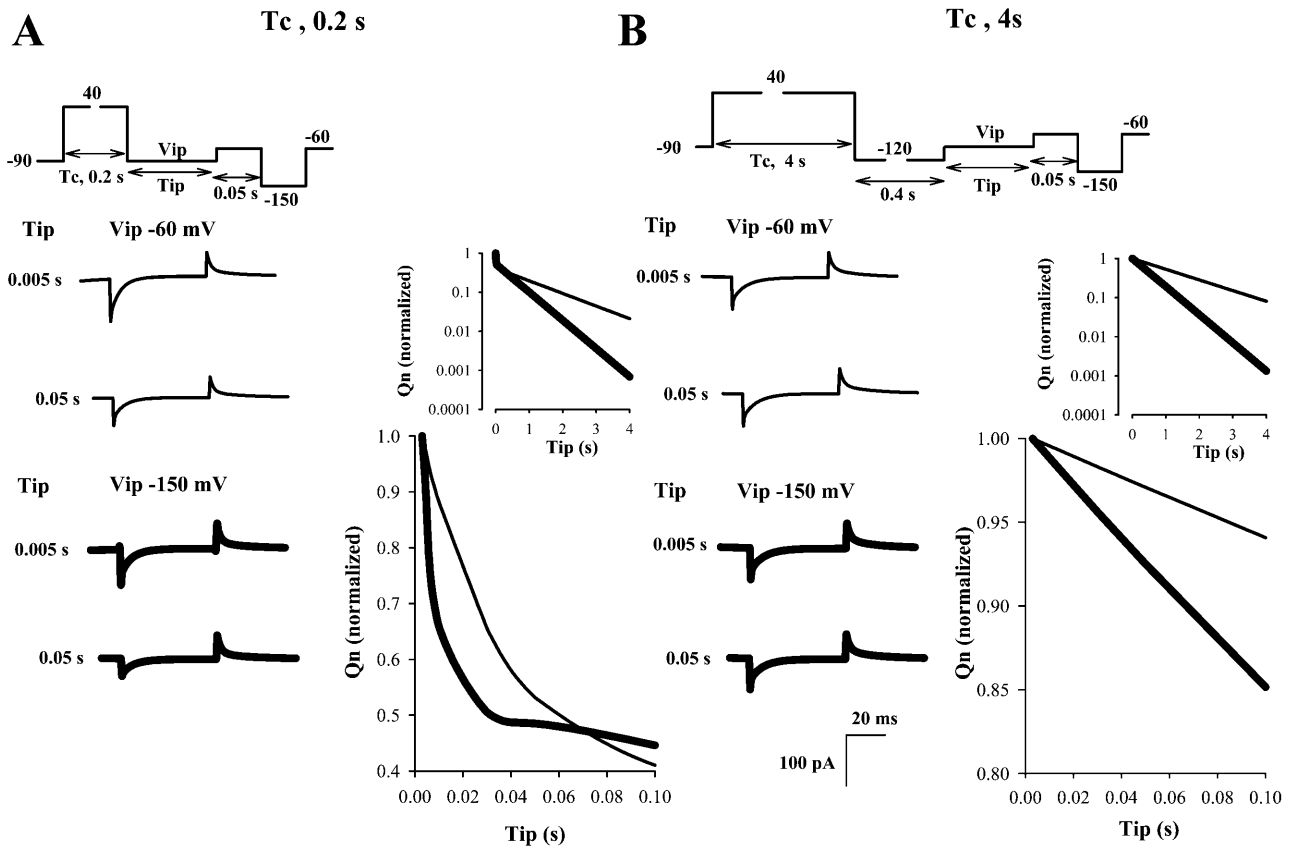


FIGURE 12 Simulated recovery from fast or slow VDI. (*A*) Recovery from fast VDI. (*Left*) Protocol (*top*) and simulated traces (*bottom*) obtained with the nine-state model with the same parameters used for Fig. 11. To induce fast VDI, $T_C$ was 0.2 s, a value similar to $\tau_f$. (*Right*) $Qn_{ON}$ / initial $Qn_{ON}$ versus *Tip*. At either *Vip* (−60 or −150 mV), the time course of recovery was well-described as the sum of two exponentials (see *semilog plot* in *inset*). The fast component of recovery was hastened at the more negative *Vip* ($\tau_{fast}$ went from 32 to 5 ms). (*B*) Recovery from slow VDI. (*Left*) Protocol (*top*) and simulated traces (*bottom*). Same parameter values as in Fig. 11. A 0.4-s sojourn at −120 mV was intercalated to recover from fast VDI. $T_C$ was 4 s (similar to Fig. 8, ~2–3 $\tau_s$). (*Right*) $Qn_{ON}$ normalized to initial $Qn_{ON}$ (taken after the 0.4-s pulse to recover from fast VDI). At either *Vip*, the time course of recovery was well-described by a single exponential (see *inset*). $\tau_s$ went from 1.3 at $Vip = -60$ mV to 0.6 s at −150 mV.

VDI is modulated by a binding site possibly located in the extracellular mouth or the pore of the channel. Upon binding of divalent (or trivalent) cations, conformational changes in the structures responsible for fast VDI can take place. Intracellular accessibility of the pore and docking by an intracellular inactivating particle might be enhanced. A possible relationship between occupancy of regions related to the $Ca^{2+}$ channel pore by blocking drugs and inactivation has been suggested (Hering et al., 1998). Ion requirements of fast VDI reported here agree with those considerations, suggesting that the outer vestibule or external pore has critical regions related to fast VDI (Hering et al., 1998; Berjukow et al., 2000; Berjukow and Hering, 2001; Sokolov et al., 2001). A possible docking site for the inactivating particle of fast VDI could be IS6, as this region is part of the pore structure and has been implicated in voltage-dependent inactivation of $Ca^{2+}$ channels (Zhang et al., 1994). This mechanism works in an opposite way to other examples where extracellular cations modulate inactivation (''priming site'' in the DHP receptor in skeletal muscle, see Brum et al., 1988; C-type inactivation, see Baukrowitz and Yellen, 1995). Whereas site occupancy opposes C-type inactivation in *Shaker* $K^+$ channels or in the DHP receptor of skeletal muscle, fast VDI of the cardiac $Ca^{2+}$ channel is promoted by occupancy of the site. Recently, Sun et al. (2000) proposed that divalent cations antagonize VDI in L-type $Ca^{2+}$ channels of rat ventricular myocytes. The comparison of the onset of *Qn* in $Li^+$ and in $Gd^{3+}$ plus $Ca^{2+}$ (or $Ca^{2+}$ alone, data not shown), is in contrast with this view (see Fig. 10 *B*). In summary, the specific ionic requirements of fast VDI reported in this article can be the starting point for future structure-function studies regarding fast VDI in $Ca_v1.2$ channels.

The fast inactivation component resembles fast VDI in voltage-dependent $Na^+$ and $K^+$ channels. A possible speculative interpretation of this analogy, in agreement with other suggestions reported before (Bernatchez et al., 1998; Ferreira et al., 1999; Stotz and Zamponi, 2001a), is that there could be a hinged-lid mechanism in L-type $Ca^{2+}$ channels. That intracellular trypsin removes inactivation of L-type

channels (Hescheler and Trautwein, 1988; Obejero-Paz et al., 1991; Klockner et al., 1995; Schmid et al., 1995), also agrees with this idea. Putative locations for a hinged lid are intracellular regions of the $\alpha$1 subunit (I–II linker or C-terminal region; see Hering et al., 2000; Stotz and Zamponi, 2001a,b). It has been suggested that the $\beta$2a subunit might interfere with a hinged lid (Restituito et al., 2000; Stotz and Zamponi, 2001b). Against this possibility, the present results show that fast VDI still takes place with $\beta$2a.

### Relationship with other inactivation mechanisms described in $Ca_v1.2$

Fast and slow VDI could be considered analogous to a modal gating, where internal horizontal transitions are far more frequent than those between the horizontal pathways. Fast VDI could arise from mode I, whereas slow VDI from mode II (Pietrobon and Hess, 1990). In this view, agents that modulate interconversion of modes should change the relative weight of the kinetic components of VDI. Experiments at the level of single channel in the time range of the kinetic components will contribute to elucidate the relationship between modes of gating and the kinetic components of inactivation.

The ''classical'' view regarding the relationship between CDI and VDI, is that CDI does not influence VDI (Hadley and Lederer, 1991; Shirokov et al., 1993). However, recent reports suggest that VDI might be affected by high intracellular $Ca^{2+}$ (Ferreira et al., 1998; Shirokov, 1999; Isaev et al., 2002). VDI does not require CDI or the ions that determine it, because fast VDI is seen when the channel is blocked. However, the rate of fast VDI might be modulated by CDI. The putative gates affecting fast VDI or CDI would work once the channel is open. The modulation could arise by interaction of the respective conformational changes of CDI and VDI. Alternatively, fast VDI might be directly modulated by the same ions that cause CDI. If this was the case, the differences between these mechanisms should be related to the degree of ion sensitivity of the sites (much lower for fast VDI than for CDI). Future experiments will clarify the basis and extent of the interaction between fast VDI and CDI.

### Implications for charge immobilization in other channels

Charge immobilization in voltage-dependent channels is usually associated with fast voltage-dependent inactivation mechanisms. Immobilization of gating charge results from block or occlusion of the intracellular mouth of the channel by a cytoplasmic moiety, envisioned as a tethered particle. Though generally accepted, this type of interpretation applies better to the inactivating *Shaker* $K^+$ channel than to the $Na^+$ channel for which it was originally proposed (Bezanilla, 2000). The results regarding fast VDI reported in this article also lead to several questions regarding a possible generalization of such a mechanism in voltage-dependent channels. If fast VDI in $Ca_v1.2$ is due to charge immobilization as we propose in this article, then the comparison with known mechanisms of such type in $Na^+$ and $K^+$ voltage-dependent channels becomes especially interesting. The differences in kinetics and modulation by extracellular ions among them are particularly striking. Based on these analogies and differences, one plausible speculation is that the general scheme of immobilization of gating charge by an intracellular particle may be widespread among voltage-dependent channels, although the particular environment of each channel is what determines the final outcome of the interactions between tethered particle and pore. There have been several reports regarding the influence of extracellular ions in recovery from fast inactivation (Armstrong and Bezanilla, 1977; Demo and Yellen, 1991; Roux et al., 1998; Yellen, 1998; Bezanilla, 2000). The results presented here suggest that extracellular ions may also modulate charge immobilization in voltage-dependent $Na^+$ and $K^+$ channels.

The tsA201 cell lines were a gift of Dr. M. M. Hosey, of Northwestern University, Chicago, Illinois. The L-type $Ca^{2+}$ channels cDNA sequences were gifts of Drs. E. Perez-Reyes, of Loyola University, Maywood, Illinois, and Dr. M. M. Hosey. We thank the continuous support, encouragement, and discussions of Drs. Gustavo Brum and Gonzalo Pizarro. We thank J. Yi for participating in the initial stages of this work supplying transfected cells, and we also thank Dr. A. González for very helpful discussions and support throughout the development of this article. Support given by Drs. L. Salkoff, R. Latorre, C. Gonzalo, C. Caputo, and CECS is gratefully acknowledged. Centro de Estudios Cientifícos (CECS) is a Millenium Science Institute and is funded in part by grants from the Fundación Andes and the Tinker Foundation.

This work was supported by National Institutes of Health grant AR 2808 to E.R. and by Third World Academy of Sciences grant 99-301 to G.F.

## REFERENCES

Armstrong, C. M., and F. Bezanilla. 1977. Inactivation of the sodium channel. II. Gating current experiments. *J. Gen. Physiol.* 70:567–590.

Baukrowitz, T., and G. Yellen. 1995. Modulation of $K^+$ current by frequency and external $[K^+]$: a tale of two inactivation mechanisms. *Neuron.* 15:951–960.

Berjukow, S., and S. Hering. 2001. Voltage-dependent acceleration of Ca(v)1.2 channel current decay by (+)- and (−)-isradipine. *Br. J. Pharmacol.* 133:959–966.

Berjukow, S., R. Marksteiner, F. Gapp, M. J. Sinnegger, and S. Hering. 2000. Molecular mechanism of calcium channel block by isradipine. Role of a drug-induced inactivated channel conformation. *J. Biol. Chem.* 275:22114–22120.

Bernatchez, G., D. Talwar, and L. Parent. 1998. Mutations in the EF-hand motif impair the inactivation of barium currents of the cardiac $\alpha$1C channel. *Biophys. J.* 75:1727–1739.

Bezanilla, F. 2000. The voltage sensor in voltage-dependent ion channels. *Physiol. Rev.* 80:555–592.

Bezanilla, F., E. Perozo, D. M. Papazian, and E. Stefani. 1991. Molecular basis of gating charge immobilization in Shaker potassium channels. *Science.* 254:679–683.

Bezanilla, F., R. E. Taylor, and J. Fernandez. 1982. Distribution and kinetics of membrane dielectric polarization. I. Long-term inactivation of gating currents. *J. Gen. Physiol.* 79:21–40.

Bickel, B. A., and K. A. Doksum. 1977. Mathematical Statistics: Basic Ideas and Selected Topics. Holden-Day, Inc., Oakland, CA.

Boyett, M. R., H. Honjo, S. M. Harrison, W.-J. Zang, and M. S. Kirby. 1994. Ultra-slow voltage-dependent inactivation of the calcium current in guinea-pig and ferret ventricular myocytes. *Pflugers Arch.* 428:39–50.

Brum, G., R. Fitts, G. Pizarro, and E. Ríos. 1988. Voltage sensors of the frog skeletal muscle membrane require calcium to function in excitation-contraction coupling. *J. Physiol. (Lond.).* 398:475–505.

Brum, G., and E. Rios. 1987. Intramembrane charge movement in frog skeletal muscle fibres. Properties of Charge 2. *J. Physiol. (Lond.).* 387:489–517.

Cens, T., S. Restituito, S. Galas, and P. Charnet. 1999. Voltage and calcium use the same molecular determinants to inactivate calcium channels. *J. Biol. Chem.* 274:5483–5490.

Cox, D. H., and K. Dunlap. 1994. Inactivation of N-type calcium current in chick sensory neurons: calcium and voltage dependence. *J. Gen. Physiol.* 104:311–336.

De Biasi, M., H. A. Hartmann, J. A. Drewe, M. Taglialatela, A. M. Brown, and G. E. Kirsch. 1993. Inactivation determined by a single site in $K^+$ pores. *Pflugers Arch.* 422:354–363.

Demo, S. D., and G. Yellen. 1991. The inactivation gate of the Shaker $K^+$ channel behaves like an open-channel blocker. *Neuron.* 7:743–753.

Eaholtz, G., T. Scheuer, and W. A. Catterall. 1994. Restoration of inactivation and block of open sodium channels by an inactivation gate peptide. *Neuron.* 12:1041–1048.

Erickson, M. G., B. A. Alseikhan, B. Z. Peterson, and D. T. Yue. 2001. Preassociation of calmodulin with voltage-gated $Ca(^{2+})$ channels revealed by FRET in single living cells. *Neuron.* 31:973–985.

Ferreira, G., P. Artigas, G. Pizarro, and G. Brum. 1997a. Butanedione monoxime promotes voltage-dependent inactivation of L-type calcium channels in heart. Effects on gating currents. *J. Mol. Cell. Cardiol.* 29: 777–787.

Ferreira, G., H. Takeshima, E. Rios, and A. González. 1998. High intracellular calcium affects L-type calcium channel gating. *Biophys. J.* 74:A101.

Ferreira, G., J. Yi, and E. Ríos. 1999. Fast and slow components of voltage-dependent inactivation in L-type $Ca^{2+}$ channels. *Biophys. J.* 76:A340.

Ferreira, G., J. Yi, E. Rios, and R. Shirokov. 1997b. Ion-dependent inactivation of barium current through L-type calcium channels. *J. Gen. Physiol.* 109:449–461.

Hadley, R. W., and J. R. Hume. 1987. An intrinsic potential-dependent inactivation mechanism associated with calcium channels in guinea-pig myocytes. *J. Physiol. (Lond.).* 389:205–222.

Hadley, R. W., and W. J. Lederer. 1991. $Ca^{2+}$ and voltage inactivate $Ca^{2+}$ channels in guinea-pig ventricular myocytes through independent mechanisms. *J. Physiol. (Lond.).* 444:257–268.

Hering, S., S. Berjukow, S. Aczel, and E. N. Timin. 1998. $Ca^{2+}$ channel block and inactivation: common molecular determinants. *Trends Pharmacol. Sci.* 19:439–443.

Hering, S., S. Berjukow, S. Sokolov, R. Marksteiner, R. G. Weiss, R. Kraus, and E. N. Timin. 2000. Molecular determinants of inactivation in voltage-gated $Ca^{2+}$ channels. *J. Physiol. (Lond.).* 528:237–249.

Hescheler, J., and W. Trautwein. 1988. Modification of L-type calcium current by intracellularly applied trypsin in guinea-pig ventricular myocytes. *J. Physiol. (Lond.).* 404:259–274.

Hess, P., J. Lansman, and R. W. Tsien. 1986. Calcium channel selectivity for divalent and monovalent cations. Voltage and concentration dependence of single channel current in ventricular heart cells. *J. Gen. Physiol.* 88:293–319.

Hoshi, T., W. N. Zagotta, and R. W. Aldrich. 1990. Biophysical and molecular mechanisms of *Shaker* potassium channel inactivation. *Science.* 250:533–538.

Hoshi, T., W. N. Zagotta, and R. W. Aldrich. 1991. Two types of inactivation in *Shaker* $K^+$ channels: effects of alterations in the carboxy-terminal region. *Neuron.* 7:547–556.

Isaev, D., K. Solt, and R. Shirokov. 2002. Gating of $CA_v1.2$ channels in high intracellular calcium: evidence for a unified theory of inactivation. *Biophys. J.* 82:A99.

Josephson, I. 1996. Depolarization shifts the voltage dependence of cardiac sodium channel and calcium channel gating charge movements. *Pflugers Arch.* 431:895–904.

Kass, R. S., and M. C. Sanguinetti. 1984. Inactivation of calcium channel current in the calf cardiac Purkinje fiber. *J. Gen. Physiol.* 84:705–726.

Kay, A. R. 1991. Inactivation kinetics of calcium current of acutely dissociated CA1 pyramidal cells of the mature guinea-pig hippocampus. *J. Physiol. (Lond.).* 437:27–48.

Klemic, K. G., G. E. Kirsch, and S. W. Jones. 2001. U-type inactivation of Kv3.1 and *Shaker* potassium channels. *Biophys. J.* 81:814–826.

Klockner, U., G. Mikala, M. Varadi, G. Varadi, and A. Schwartz. 1995. Involvement of the carboxyl-terminal region of the $\alpha 1$ subunit in voltage-dependent inactivation of cardiac calcium channels. *J. Biol. Chem.* 270:17306–17310.

Kuo, C. C., and B. P. Bean. 1994. $Na^+$ channels must deactivate to recover from inactivation. *Neuron.* 12:819–829.

Loots, E., and E. Y. Isacoff. 1998. Protein rearrangements underlying slow inactivation of the *Shaker* $K^+$ channel. *J. Gen. Physiol.* 112:377–389.

Lopez-Barneo, J., T. Hoshi, S. Heinemann, and R. W. Aldrich. 1993. Effects of external cations and mutations in the pore region on C-type inactivation of *Shaker* potassium channels. *Receptors Channels.* 1:61–71.

Marks, T. N., and S. W. Jones. 1992. Calcium currents in the A7r5 smooth muscle-derived cell line. An allosteric model for calcium channel activation and dihydropyridine agonist action. *J. Gen. Physiol.* 99: 367–390.

Markwardt, F., and B. Nilius. 1988. Modulation of calcium channel currents in guinea-pig single ventricular heart cells by the dihydropyridine Bay K 8644. *J. Physiol. (Lond.).* 399:559–575.

Mazzanti, M., L. J. DeFelice, and Y. M. Liu. 1991. Gating of L-type $Ca^{2+}$ channels in embryonic chick ventricle cell: dependence on voltage, current and channel density. *J. Physiol. (Lond.).* 443:307–344.

McDonald, T. F., S. Pelzer, W. Trautwein, and D. J. Pelzer. 1994. Regulation and modulation of calcium channels in cardiac, skeletal, and smooth muscle cells. *Physiol. Rev.* 74:365–507.

Mouton, J., A. Feltz, and Y. Maulet. 2001. Interactions of calmodulin with two peptides derived from the C-terminal cytoplasmic domain of the Ca(v)1.2 $Ca^{2+}$ channel provide evidence for a molecular switch involved in $Ca^{2+}$-induced inactivation. *J. Biol. Chem.* 276:22359–22367.

Nilius, B., K. Kitamura, and H. Kuriyama. 1994. Properties of inactivation of calcium channel currents in smooth muscle cells of rabbit portal vein. *Pflugers Arch.* 426:239–246.

Obejero-Paz, C. A., S. W. Jones, and A. Scarpa. 1991. Calcium currents in the A7r5 smooth muscle-derived cell line. Increase in current and selective removal of voltage-dependent inactivation by intracellular trypsin. *J. Gen. Physiol.* 98:1127–1140.

Olcese, R., R. Latorre, L. Toro, F. Bezanilla, and E. Stefani. 1997. Correlation between charge movement and ionic current during slow inactivation in *Shaker* $K^+$ channels. *J. Gen. Physiol.* 110:579–589.

Ong, B. H., G. F. Tomaselli, and J. R. Balser. 2000. A structural rearrangement in the sodium channel pore linked to slow inactivation and use dependence. *J. Gen. Physiol.* 116:653–662.

Peterson, B. Z., C. D. DeMaria, J. P. Adelman, and D. T. Yue. 1999. Calmodulin is the $Ca^{2+}$ sensor for $Ca^{2+}$ -dependent inactivation of L-type calcium channels. *Neuron.* 22:549–558.

Peterson, B. Z., J. S. Lee, J. G. Mulle, Y. Wang, M. de Leon, and D. T. Yue. 2000. Critical determinants of $Ca(^{2+})$-dependent inactivation within an EF-hand motif of L-type $Ca(^{2+})$ channels. *Biophys. J.* 78:1906–1920.

Pietrobon, D., and P. Hess. 1990. Novel mechanism of voltage-dependent gating in L-type calcium channels. *Nature.* 346:651–655.

Qin, N., R. Olcese, M. Bransby, T. Lin, and L. Birnbaumer. 1999. $Ca^{2+}$-induced inhibition of the cardiac $Ca^{2+}$ channel depends on calmodulin. *Proc. Natl. Acad. Sci. USA.* 96:2435–2438.

Restituito, S., T. Cens, C. Barrere, S. Geib, S. Galas, M. De Waard, and P. Charnet. 2000. The $\beta$2a subunit is a molecular groom for the $Ca^{2+}$ channel inactivation gate. *J. Neurosci.* 20:9046–9052.

Roux, M. J., R. Olcese, L. Toro, F. Bezanilla, and E. Stefani. 1998. Fast inactivation in *Shaker* $K^+$ channels. Properties of ionic and gating currents. *J. Gen. Physiol.* 111:625–638.

Schmid, R., K. Seydl, W. Baumgartner, K. Groschner, and C. Romanin. 1995. Trypsin increases availability and open probability of cardiac L-type $Ca^{2+}$ channels without affecting inactivation induced by $Ca^{2+}$. *Biophys. J.* 69:1847–1857.

Shirokov, R. 1999. Interaction between permeant ions and voltage sensor during inactivation of N-type $Ca^{2+}$ channels. *J. Physiol. (Lond.).* 518:697–703.

Shirokov, R., G. Ferreira, J. Yi, and E. Rios. 1998. Inactivation of gating currents of L-type calcium channels. Specific role of the $\alpha 2\delta$ subunit. *J. Gen. Physiol.* 111:807–823.

Shirokov, R., R. Levis, N. Shirokova, and E. Ríos. 1992. Two classes of gating current from L-type Ca channels in guinea pig ventricular myocytes. *J. Gen. Physiol.* 99:863–895.

Shirokov, R., R. Levis, N. Shirokova, and E. Ríos. 1993. $Ca^{2+}$-dependent inactivation of cardiac L-type $Ca^{2+}$ channels does not affect their voltage sensor. *J. Gen. Physiol.* 102:1005–1030.

Sokolov, S., E. Timin, and S. Hering. 2001. On the role of $Ca(^{2+})$- and voltage-dependent inactivation in Ca(v)1.2 sensitivity for the phenylalkylamine (−)gallopamil. *Circ. Res.* 89:700–708.

Starkus, J. G., and M. D. Rayner. 1991. Gating current ''fractionation'' in crayfish giant axons. *Biophys. J.* 60:1101–1119.

Stotz, S. C., J. Hamid, R. L. Spaetgens, S. E. Jarvis, and G. W. Zamponi. 2000. Fast inactivation of voltage-dependent calcium channels. A hinged-lid mechanism? *J. Biol. Chem.* 275:24575–24582.

Stotz, S. C., and G. W. Zamponi. 2001a. Structural determinants of fast inactivation of high voltage-activated $Ca(^{2+})$ channels. *Trends Neurosci.* 24:176–181.

Stotz, S. C., and G. W. Zamponi. 2001b. Identification of inactivation determinants in the domain IIS6 region of high voltage-activated calcium channels. *J. Biol. Chem.* 276:33001–33010.

Sun, L., J. S. Fan, J. W. Clark, and P. T. Palade. 2000. A model of the L-type $Ca^{2+}$ channel in rat ventricular myocytes: ion selectivity and inactivation mechanisms. *J. Physiol.* 529:139–158.

Vilin, Y. Y., N. Makita, A. L. George, Jr., and P. C. Ruben. 1999. Structural determinants of slow inactivation in human cardiac and skeletal muscle sodium channels. *Biophys. J.* 77:1384–1393.

Yellen, G. 1998. The moving parts of voltage-gated ion channels. *Q. Rev. Biophys.* 31:239–295.

Yellen, G., D. Sodickson, T. Y. Chen, and M. E. Jurman. 1994. An engineered cysteine in the external mouth of a $K^+$ channel allows inactivation to be modulated by metal binding. *Biophys. J.* 66:1068–1075.

Zhang, J.-F., P. Ellinor, R. Aldrich, and R. Tsien. 1994. Molecular determinants of voltage-dependent inactivation in calcium channels. *Nature.* 372:97–100.

Zuhlke, R. D., G. S. Pitt, K. Deisseroth, R. W. Tsien, and H. Reuter. 1999. Calmodulin supports both inactivation and facilitation of L-type calcium channels. *Nature.* 399:159–162.